

2010

## Enhancement Of Jet Impingement Heat Transfer Using Shape Modification And Phase Change

Yacob Mesfin Argaw  
*North Carolina Agricultural and Technical State University*

Follow this and additional works at: <https://digital.library.ncat.edu/theses>

---

### Recommended Citation

Argaw, Yacob Mesfin, "Enhancement Of Jet Impingement Heat Transfer Using Shape Modification And Phase Change" (2010). *Theses*. 21.  
<https://digital.library.ncat.edu/theses/21>

This Thesis is brought to you for free and open access by the Electronic Theses and Dissertations at Aggie Digital Collections and Scholarship. It has been accepted for inclusion in Theses by an authorized administrator of Aggie Digital Collections and Scholarship. For more information, please contact [iyanna@ncat.edu](mailto:iyanna@ncat.edu).

ENHANCEMENT OF JET IMPINGEMENT HEAT TRANSFER USING SHAPE  
MODIFICATION AND PHASE CHANGE

by

Yacob Mesfin Argaw

A thesis submitted to the graduate faculty  
in partial fulfillment of the requirements for the degree of  
MASTER OF SCIENCE

Department: Mechanical Engineering  
Major: Mechanical Engineering  
Major Professor: Dr. John P. Kizito

North Carolina A&T State University  
Greensboro, North Carolina  
2010

School of Graduate Studies  
North Carolina Agricultural and Technical State University

This is to certify that the Master's Thesis of

Yacob Mesfin Argaw

has met the thesis requirements of  
North Carolina Agricultural and Technical State University

Greensboro, North Carolina  
2010

Approved by:

---

Dr. John P. Kizito  
Major Professor

---

Dr. DeRome Dunn  
Committee Member

---

Dr. Vinayak N. Kabadi  
Committee Member

---

Dr. Samuel P. Owusu-Ofori  
Department Chairperson

---

Dr. Alan Letton  
Interim Associate Vice Chancellor for  
Research and Graduate Dean

Copyright by  
YACOB MESFIN ARGAW  
2010

## **BIOGRAPHICAL SKETCH**

Yacob Mesfin Argaw was born on June 11, 1981 in Addis Ababa, Ethiopia. Yacob Mesfin Argaw received the Bachelor of Science degree in Mechanical Engineering from Addis Ababa University, Faculty of Technology in 2005. Subsequent to graduation, being one of the highest ranking students in the batch, Yacob Mesfin Argaw was offered an opportunity by the same university to lecture in the department. For three years Yacob worked at Addis Ababa University, Mechanical Engineering Department at the rank of Assistant Lecturer until North Carolina Agricultural and Technical State University Mechanical Engineering Department offered him an assistantship to pursue his Masters study. Yacob Mesfin Argaw is a candidate for the Master of Science in Mechanical Engineering at North Carolina Agricultural and Technical State University in Greensboro, North Carolina.

## **ACKNOWLEDGMENTS**

I thank God for the life He has given me so that I may appreciate His gifts and live life to the fullest. I also express my immense gratitude to Dr. John P. Kizito for his unparalleled support in funding my study and his continual guidance while working on this thesis. He always sheds some light on things when they get confusing. To my friends in and outside the lab, I appreciate your help and friendship. I thank the Air Force Research Laboratory (AFRL) at Dayton Ohio (US DoD) for funding this research.

## TABLE OF CONTENTS

LIST OF FIGURES .....	viii
LIST OF TABLES .....	x
NOMENCLATURE.....	xi
ABSTRACT .....	xiv
CHAPTER 1. INTRODUCTION .....	1
1.1. Specific Objectives .....	2
1.2. Practical Significance .....	3
CHAPTER 2. LITERATURE REVIEW .....	5
2.1. Cooling Requirements .....	5
2.2. High Rate Heat Transfer Techniques .....	6
2.3. Effective Range of Cooling Techniques.....	8
2.4. Phase Change .....	9
2.5. Bubble Formation.....	11
2.6. Bubble Collapse Creating Additional Turbulence .....	12
2.7. Impinging Jets .....	13
2.8. Advantages and Disadvantages of Jet and Spray Cooling .....	16
2.9. Droplet Dynamics.....	16
2.10. Droplet Sound .....	18
2.11. Factors Influencing Heat Transfer .....	19
2.11.1. Confinement .....	19

2.11.2.	Nozzles and Jet-to-Target Spacing .....	20
2.11.3.	Fluid Types.....	21
2.11.4.	Nozzle Geometry, Angle, and Inclination.....	21
2.11.5.	Nozzle Configurations and Outlet Design .....	23
2.11.6.	Dimensionless Parameters .....	25
2.11.7.	System Parameters .....	26
2.12.	Literature Review Conclusion .....	28
CHAPTER 3. PROBLEM FORMULATION AND METHODOLOGY.....		29
3.1.	Jet Impingement without Phase Change.....	29
3.1.1.	Single Phase Modeling Process .....	36
3.1.2.	Gravity Effect on Jet Impingement .....	37
3.2.	Phase change .....	38
3.2.1.	Multiphase Modeling Process.....	40
3.2.2.	Gravity Effect on Phase Change .....	51
3.3.	Grid Independence Study .....	53
CHAPTER 4. RESULTS.....		56
4.1.	Results of Optimum Shape Search.....	56
4.2.	Results of Phase Change Jet Impingement.....	67
CHAPTER 5. CONCLUSION.....		72
REFERENCES .....		74
APPENDIX A. PHASE CHANGE HEAT TRANSFER THEORY.....		80
APPENDIX B. DIFFERENT IMPINGEMENT SURFACES .....		83



## LIST OF FIGURES

FIGURES	PAGE
1. Boiling curve for saturated liquid .....	7
2. Variation of achievable surface heat flux for various heat transfer modes against temperature difference .....	9
3. Effect of evaporation at point A, in (a) and (b) leads to change in curvature shown in (c) and (d) at the TPL .....	12
4. Regions on the target surface due to an impinging circular jet .....	14
5. Schematics of (a) Free surface (b) Plunging (c) Submerged (d) Confined and (e) Wall impingement configurations .....	15
6. Phase change in light sprays .....	17
7. Simplified Heating Chamber Model .....	30
8. Boundary layer on flow over a wedge.....	32
9. 3D simulation of particle pathlines upon impingement.....	33
10. Plot of (a) Velocity Vector and (b) Temperature contour of initial simulation model.....	34
11. Schematic of representative model used in simulation.....	35
12. Phase change line on enthalpy–temperature graph.....	47
13. Plot of residuals .....	55
14. Bar chart of enhancement for different models .....	57
15. Plot of surface (a) Temperature and (b) Heat Flux versus Wedge Angles .....	58
16. Velocity vector, pressure contour and static temperature plots of (a and b) A-type model, (c and d) V-type model, and (e) flat surface model at 10 sececond time elapse.....	60

17. Surface temperature profile comparison of models after 10 second real time simulation elapse.....	61
18. Heat Flux comparison of models analyzed at 10 second time elapse .....	62
19. Surface heat flux comparison of Modified shapes with flat surface .....	63
20. VA-type mode .....	64
21. Heat flux comparison with the new model .....	64
22. Heat Flux Comparison of the newVA-type models.....	65
23. Plot of velocity, pressure and temperature for (a) VA2-type (b) VA1-type and (c) VA-Flat models .....	66
24. Convergence history of Volume-Average Volume fraction of vapor .....	68
25. Convergence history of Area-Weighted Average Surface Nusselt Number.....	68
26. Temperature comparison for phase change models with and without jet impingement.....	69
27. Surface Heat Flux comparison.....	69
28. Surface Nusselt Number comparison .....	70
29. Contours of volume fraction of vapor (a) t=3sec, (b) t =4sec, and (c) t=5sec for pool phase change model (left) and jet impingment model with jet velocity of 2 m/s (right).....	71

## LIST OF TABLES

<b>TABLES</b>	<b>PAGE</b>
1. Effect of system parameters on phase change heat transfer .....	27
2. Description of modeling parameters for jet impingement simulation.....	33
3. Model half wedge angles.....	36
4. Description of modeling parameters for phase change simulation. ....	40
5. Material properties of two phase flow fluids .....	43
6. Minimum time step determination technique .....	44
7. Boundary conditions available for a multiphase model .....	50
8. Input parameters for modeling.....	52
9. Grid independence study maximum temperature taken as the variable .....	54
10. Summary of heat flux enhancement in changing the wedge angle .....	56
11. Comparison heat flux and overall enhancement of VA type model with the high performance A-type and V-type models .....	65

## NOMENCLATURE

A	heating area (m <sup>2</sup> )
Ar	Aspect ratio
CFD	computational fluid dynamics
Ca	Capillary number, $Ca = \frac{\mu U}{\sigma}$
Cp	specific heat (J/kgK)
D	nozzle diameter (m)
f	body force
H	Total enthalpy (W/m <sup>2</sup> K)
h <sub>fg</sub>	latent heat of vaporization (J/kg)
k	thermal conductivity
L	characteristic length
La	Laplace number, $La = \frac{\rho \sigma D}{\mu^2}$
L/D	nozzle length to diameter ratio
X/d, H/d	ratio of nozzle to surface distance to nozzle diameter
Nu	local Nusselt number
Nu <sub>ave</sub>	average Nusselt number
P	pressure (Pa)
Pr	Prandtl number $Pr = c_{p,air} \mu_{air} / k_{air}$
q <sub>c</sub>	convection heat flux, (W/m <sup>2</sup> )

$Q_{\text{cond}}$	conduction heat transfer rate, (W)
$Q_e$	evaporative heat flux (W)
$Q$	total dissipation power, (W)
$Re$	Reynolds number, $Re = \frac{\rho Du}{\mu}$
$S$	Source term
$t$	time (s)
$T$	temperature (K)
$T_{\text{sat}}$	Saturation temperature, ( $^{\circ}\text{C}$ )
$T_{\infty}$	ambient temperature (K)
$u, v, w$	velocity components in x, y, z directions (m)
$U$	jet inlet velocity, (m/s)
$V$	Volume ( $\text{m}^3$ )
$We$	Weber number, $We = \frac{\rho LU^2}{\sigma}$

### GREEK SYMBOLS

$\rho$	density, ( $\text{kg}/\text{m}^3$ )
$\nu$	kinematic viscosity, ( $\text{m}^2/\text{s}$ )
$\mu$	dynamic viscosity, ( $\text{kg}/\text{ms}$ )
$\tau$	Stress Tensor
$\beta, \alpha$	Wedge angles
$\sigma$	Surface tension
$\nabla^2$	Laplacian

**$\Delta$**             gradient

**SUBSCRIPTS**

b                bubble

l                liquid

v                vapor

sat             saturate

i                index

## ABSTRACT

**Argaw, Yacob Mesfin.** ENHANCEMENT OF JET IMPINGEMENT HEAT TRANSFER USING SHAPE MODIFICATION AND PHASE CHANGE. (**Advisor: John P. Kizito**), North Carolina Agricultural and Technical State University.

The overall goal of the present study is to enhance heat transfer rate performance on high heat flux surfaces while maintaining a uniform and low temperature of the substrate. The specific objectives are to determine shapes which maximize heat transport from heater surfaces when using jet impingement cooling method and to model a two phase jet impingement process which incorporates phase change at the impingement substrate. A very high heat flux of up to  $10\text{MW/m}^2$  is applied at the bottom of a heated chamber and a jet of air and water are applied separately to a confined control volume. Free stream flow past a heated wedge can be modeled and solved by Falkner-Skan equations when the wedge angle is within a limit. However, when the impingement surface is constrained by walls to create a cavity, the method is no longer valid.

A commercially available Computational Fluid Dynamics (CFD) code Fluent® is modified with user defined code to analyze the physical problem numerically. The results show that a newly generated impingement profile, which incorporates a wedge and a concave profile, gives the best performance. Specifically, the heat transfer enhancement level is around 20% higher when compared to a flat surface. The presence of phase change also increases the overall heat removal due to the additional latent heat of vaporization transfer through mass transport. The models developed in the study can be extended to optimize spray cooling schemes.

# CHAPTER 1

## INTRODUCTION

Industries such as material processing, manufacturing plants, power stations, laser technologies, combustion chambers, and de-icing of aircraft systems, all demand effective cooling systems to operate properly. Engineers working on design and management of thermal parts face a big challenge as they work on creating better tools while keeping the size as compact as possible. For high heat flux components, the smaller the surface area, the more difficult it becomes to cool. Therefore, cooling those components found in very high temperature environments and high heat flux transmitting parts has been an interest of many researchers.

The applications of high capacity cooling techniques improve considerably by combining two or more technological merits together to get a better thermal control and heat management. The literature review in chapter 2 presents the importance of high rate heat transfer techniques that are of interest for various industries. The maximum heat flux reported in previous research and those factors affecting heat transfer are also presented.

Bergles reported that, “about ten percent of heat transfer literature now concerns enhancement and a recent year of *Journal of Heat Transfer* has over 20 percent of the papers directed to various areas of enhancement” [1]. The statement shows how important enhancements in high rate heat transfer techniques have become. However,



after an extensive literature review presented in chapter 2, the present study concluded that there are no papers focused on improving heat transfer by macro level shape modification in jet impingement surfaces. The review shows much has been said about the effects of impingement surface roughness, finned plates and other surface parameters. Yet there are few studies performed on the effect of impingement profile in a confined heater as will be presented in the study.

### **1.1. Specific Objectives**

The motivation of the present study is based on the need derived from the Air Force Research Laboratory (AFRL) funded research to manage high heat flux producing components. An experimental setup for a cooling thermal loop that can remove a heat flux of  $10 \text{ MW/m}^2$  has been constructed by the Fluid and Thermal Management Research group. The thermal loop uses a two phase cooling scheme utilizing vapor as atomizing fluid. The heat generated by a copper heater having a crown area of  $10^{-4} \text{ m}^2$  is cooled by impinging jet methods. Specifically, as the saturated jet comes in contact with the high temperature heater surface phase change will take place.

Simulation software was used as a tool to complement experimental studies. Analysis in the present study is used to visualize flow, study the effect of parameters, analyze cause and effect and improve experimental studies. In earlier days, use of computers for solving higher order differential equations was minimal because of their computational costs. However improvements in computational capacity and processor

speed of computers make their use an essential part of the solution searching process.

The specific objectives of the present study are to:

- Determine shapes which maximize heat transport from heater surfaces when using jet impingement cooling method.
- Model a two phase jet impingement process which incorporates phase change at the impingement substrate.

## **1.2. Practical Significance**

The rationale of studying the aforementioned specific objectives is to enhance heat transfer performances of high flux surfaces. The new impingement surfaces constructed through the analysis performed in the subsequent chapters help to improve jet impingement heat effectiveness. Industries can benefit from having higher heat transfer performance in their already existing jet impingement cooling systems by making a simple modification to the heated surface. The presence of phase change along with jet impingement in a system also assists the heat transfer process by taking a huge amount of latent heat. A better heat transfer almost always results in a lower surface temperature which means extended part life.

The thesis organization is as follows: the second chapter presents the work done by others as it relates to high rate heat transfer. Advantages of specific cooling mechanisms and factors that influence heat transfer are also discussed to give a rationale for the present specific objectives. In the third chapter, the problem formulation, methodologies used, and CFD model development are discussed. Results and discussion

on the phase change jet impingement cooling scheme are discussed in chapter four. Finally, in chapter five conclusions are given and further study suggestions are proposed.

## **CHAPTER 2**

### **LITERATURE REVIEW**

#### **2.1. Cooling Requirements**

Technology advancement is being observed through improved electronic components performance and high temperature resisting machines. Parts that convert or transmit power through small volume devices have become a topic of study for a while because of their effectiveness in robotics and space technology [2]. However, maximum working temperature of parts is still the main limiting factor that hinders further improvement in the overall working efficiency of many technologies [3, 4- 6, 7].

Energy dissipation due to inefficient transmission in active components is reflected by a temperature buildup. For example, heat transmission capability of electronic devices become less effective as the working temperature increases above a certain threshold value [8]. The dissipated energy in the form of heat increases component temperature, lowers its efficiency, and eventually causes the part to fail. An urge for improving the efficiency of components and imposed environmental and economical constraints increase the need for superior heat dissipation techniques [9, 10].

For the past few years cooling of high-density thermal components has become one of the significant research areas. Numerous researchers have proposed ways of removing the excess heat. On the average more than a dozen research papers are being published annually to address this issue [11]. To date, it is generally understood that low

capacity cooling techniques are no longer reliable for heavy duty applications like: nuclear technology, aerospace components, laser technology, and cooling turbine blades [12]. Therefore the need for developing high rate heat transfer techniques makes the study worthwhile.

## **2.2. High Rate Heat Transfer Techniques**

For high performance components conduction, natural convection and radiation heat transfer mechanisms alone are unable to take away the generated/transmitted heat at an equal pace to avoid temperature build up. Therefore a special technique has to be considered if the generated heat needs to be damped at an equal rate.

One means of achieving high rate heat transfer is through the use of impinging jets. The fact that impinging fluid has a relatively higher convective heat transfer coefficient as opposed to conduction improves the heat transfer enormously. As power dissipation level increases in electronic systems and machineries liquids become more effective than air due to liquids' higher specific heat capacity. Possible liquid cooling technologies include; single-phase liquid cooling, spray cooling, jet impingement, heat pipes, and immersion flow boiling [10].

Phase change process is the other well studied high rate heat transfer technique. Earlier researchers exhaustively studied phase change process analytically and experimentally and showed phase change is indeed a more efficient heat transfer process because of the extra latent heat it dissipates [13 - 15]. Based on interactions of fluid to heated surface, phase change phenomena is illustrated in the boiling curve as shown in

Figure 1 [16]. The plot of surface heat flux,  $q''$ , against wall superheat  $\Delta T_{sub}$  (wall temperature minus saturation temperature of the liquid) is considered to be the most descriptive representation of the boiling process.

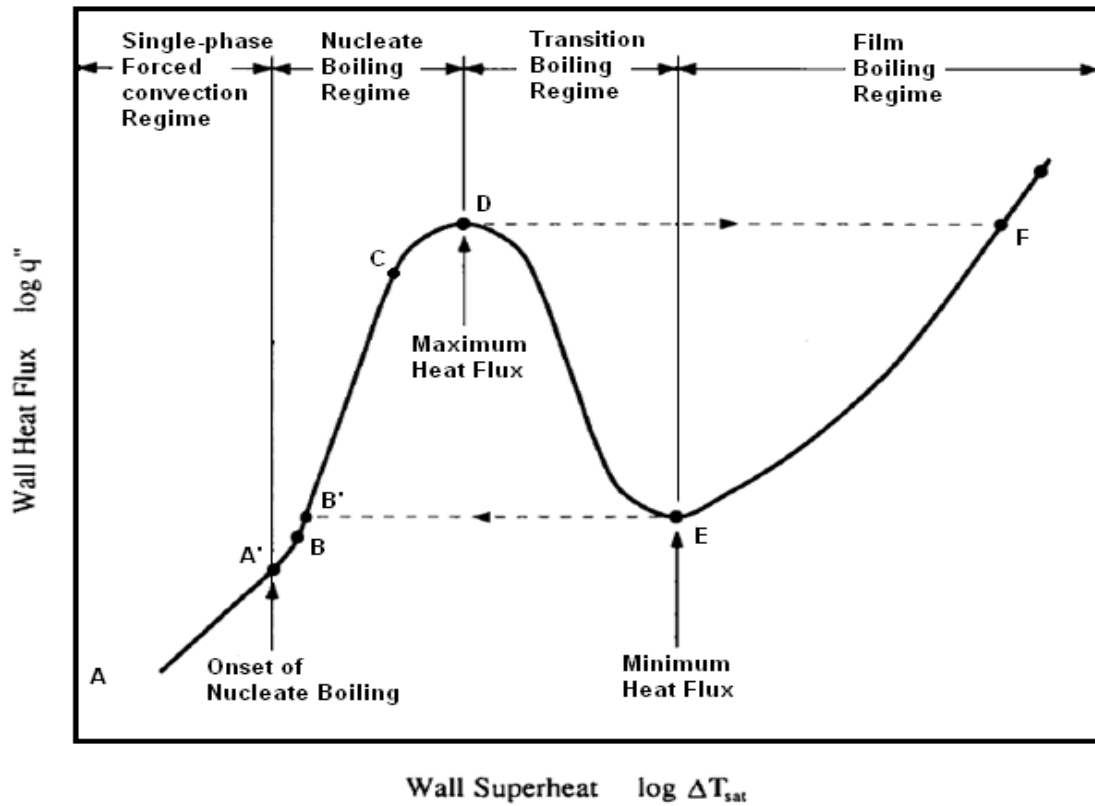


Figure 1. Boiling curve for saturated liquid [15]

Bergles et al. [1] and Monde et al. [17] have reported a blanketing effect of the generated vapor as heat flux increases the critical heat flux value. Therefore, the heated surface suffers an enormous temperature rise since the bulk fluid is hindered from

coming in contact with the surface. This is an indication that unless the process is controlled properly “thermal burnout” and material failure might result.

### **2.3. Effective Range of Cooling Techniques**

The most desirable working region of cooling components is in nucleate boiling region. Ranges of achievable surface heat flux values for different modes of heat transfer and fluid types are provided by Mal et al. shown in Figure 2 [11]. For instance, if a typical process has the maximum available temperature difference of 40K, as can be seen on the graph, natural convection air cooling is effective for  $0.5\text{kW/m}^2$  heat flux removal and forced convection with air is effective for removing heat flux up to  $2.5\text{kW/m}^2$ . However, liquid cooling modes can transport hundreds of kilowatts per square meter. This is an eye opener for understanding the effectiveness of high heat capacity coolants and phase change process.

The equation that describes the slope of mode of cooling mechanism in Figure 2 can be expressed as the ratio of the two coordinates  $q''/\Delta T$ . The rule of thumb is that, the steeper the slope the more effective, the mode of heat transfer is. For example, heat transfer coefficients for systems employing single-phase convection or impinging liquid jets is typically around  $10\text{kW/m}^2\text{-}^\circ\text{C}$  but are much larger in the presence of phase change. Even though boiling can provide removal of a large amount of heat flux over small temperature range, there are limits to the applicability and effectiveness of it which must be considered right at the design stage [18].

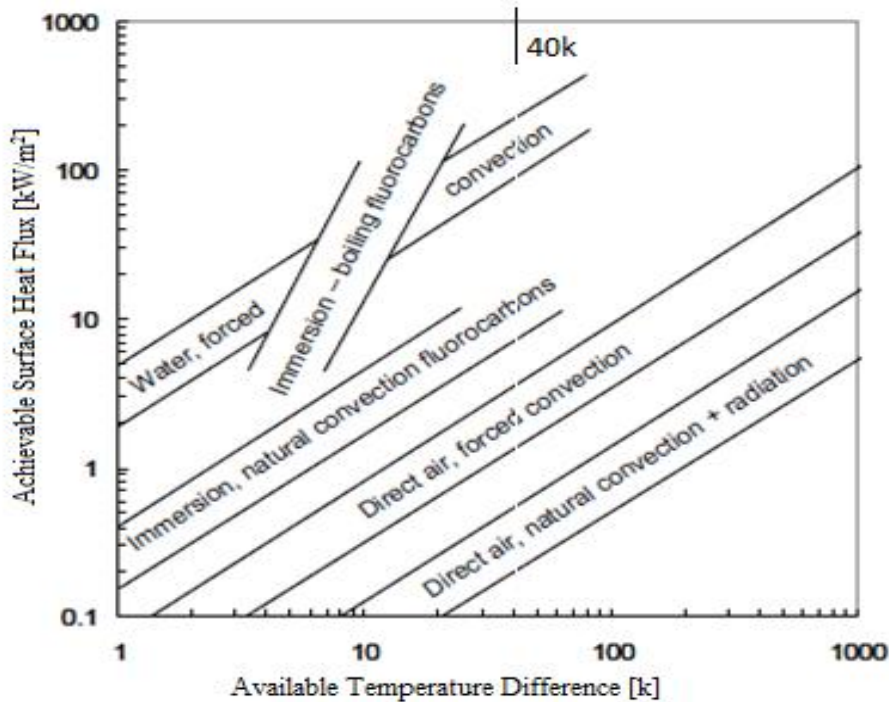


**Figure 2. Variation of achievable surface heat flux for various heat transfer modes against temperature difference [11]**

#### 2.4. Phase Change

A comprehensive literature survey, prepared in two parts by Piro et al. concerning effects of boiling surface and prediction methods to calculate the heat transfer coefficient for nucleate boiling gives a good understanding on phase change heat transfer and the parameters that affect it [4]. After reviewing around seventy papers written from 1936 through 1999, they concluded that among the major parameters affecting the heat transfer coefficient heat flux, saturation pressure, and thermo-physical properties of the working fluid (thermal conductivity and thermal absorption) have been the most investigated and well established factors.



As the heat flux on heated surface increases and more nucleation sites are generated, bubbles start detaching vigorously and lift off due to buoyancy effect. The cyclic movement due to nucleation, growth, and departure/collapse of vapor bubbles agitate the fluid near the surface. The perturbation, some literatures call it the quenching effect, is a result of liquid rushing to fill up the space left by rising bubbles. In effect the induced perturbation enhances the convective heat transfer coefficient [6, 19, and 15]. Thus according to Omar et al. [13] and Mitrovic [20] heat flux parameter in boiling comprises three components as expressed in equations 2.1 through 2.4 by Anglart et al. [17]. The total heat flux is the summation of these three components listed below,

- heat used in direct evaporation to generate bubbles,  $q_{eva}$
- heat transfer through direct contact of liquid that replaces the bubble,  $q_{qnch}$
- heat transfer through convection due to the generated wakes,  $q_{fconv}$

$$q_{tot} = q_{eva} + q_{qnch} + q_{fconv} \quad (2.1)$$

$$q_{eva} = Na \cdot f \left( \frac{\pi}{6} d_{bw}^3 \right) \rho_g h_{fg} \quad (2.2)$$

$$q_{qnch} = h_q \cdot A_{bub} (T_w - T_l) \quad (2.3)$$

$$q_{fconv} = h_{fconv} \cdot A_{fconv} (T_w - T_l) \quad (2.4)$$

where:  $d_b \approx 1.5mm$  and

$$Na = [185(T_w - T_l)]^{1.805}; \quad f = \left( \frac{4g(\rho_l - \rho_g)}{3d_{bw}\rho_l} \right)^{1/2};$$

$$h_q = \frac{1.6(q_l \rho_l C_{pl})^{1/2}}{\sqrt{0.8\pi / f}} \quad h_{fconv} = St \rho_l C_{pl} V_l$$

## 2.5. Bubble Formation

Mitrovic discussed mechanisms of bubble growth, detachment and the importance of three-phase-line (TPL) which is a point in a bubble where liquid, solid and vapor phases co-exist and interact with each other [19, 20]. Figure 3 shows that the TPL at the corner has a contact angle  $\beta$  which is a function of heat flux and wall superheat. As portion of liquid at the interface is evaporated, the TPL moves along the heated surface and this leads to an increase in the contact angle.

According to Mitrovic, evaporation along the TPL induces a number of mechanisms that act against further change of interface angle.

- Hydrodynamic effects or Marangoni flow tend to suppress formation of a convex curvature at the interface.
- Adhesion forces have a tendency to re-wet the solid surface
- Laplace pressure or surface tension force has a smoothing effect by diminishing the convex curvature.

Due to a higher heat transfer at the boundary more vapor is formed along the TPL and as a result the bubble grows rapidly. At the contact with the heated surface the vapor bubble has concave-convex curvature. As the inside radius of curvature of the interface, on the convex side, increases by bubble growth the Laplace-pressure decreases and the hydrodynamic force increases in the vapor phases. When the surplus energy reaches certain value bubble detachment process commences.

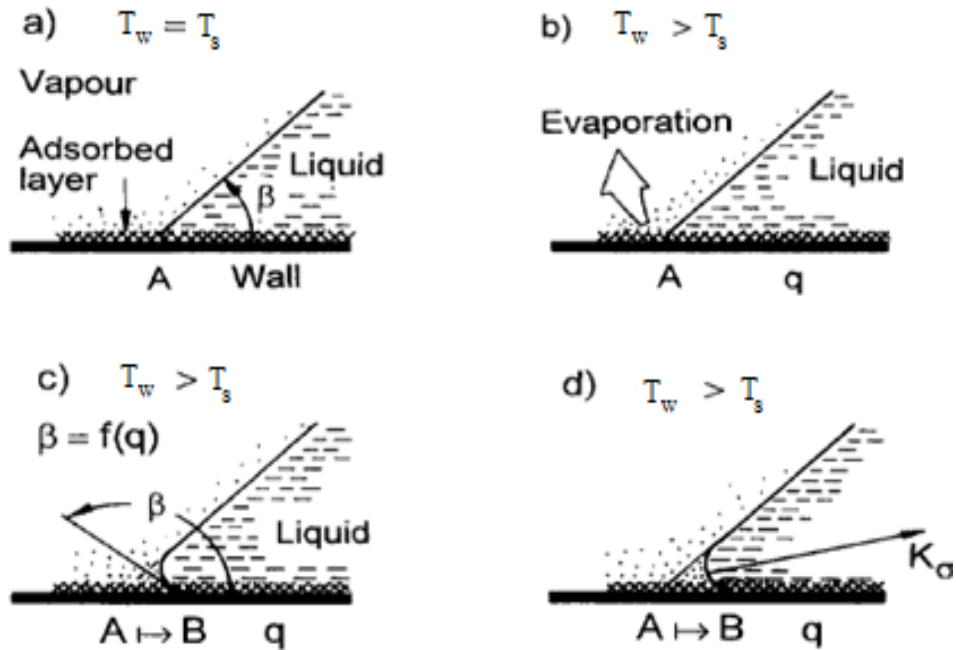


Figure 3. Effect of evaporation at point A, in (a) and (b) leads to change in curvature shown in (c) and (d) at the TPL [19]

## 2.6. Bubble Collapse Creating Additional Turbulence

Timm et al. discussed a mechanism for heat and momentum exchange between an extremely superheated wall and an impinging sub cooled water jet [21]. Bubbles of average radius  $10^{-4}$  m and life time around 0.0001 second growing and collapsing at a very close proximity of a superheated wall acts as a source of turbulence mixing. Momentum and heat exchange of the displaced fluid with the main flow results in temperature drop around the bubble which results in collapse of the bubble before detachment. Colder fluid will then fill the gap left by the burst bubble and the process will repeat itself but rather vigorously.

## 2.7. Impinging Jets

Surface impingement technique in general encompasses air/liquid jet cooling, spray cooling, and droplet impingement. Jets designed either for single nozzle or multiple nozzles, depending on their practical usefulness, have many parts and distinct working principle. Fluid gushing out of a nozzle with a relatively higher velocity than other techniques impinges on a plate placed some distance away. When the cold fluid, moving at high velocity, comes in contact with the heated surface at least two modes of heat transfer play a significant role in removing the excess heat. As a result of residence time of the liquid jet on the surface there is solid–liquid conduction that takes place and the fact that fluid moves over the surface gives convection heat transfer. If the surface temperature is extremely high phase change will occur. The additional interaction and agitation of fluid near the surface also enhances the convective heat transfer coefficient considerably. As shown in Figure 4 fluid jet impinging on a substrate is categorized into three regions based on the section in the control volume [22, 23].

The first region is the free-jet zone just out of the nozzle where the fluid moves axially. The flow gets its energy from the higher pressure that exists at the inlet. Nozzles basically work as throttling devices since they drop the pressure across them and the pressure difference gives momentum to the fluid. The second region is the impingement zone where the jet starts changing its flow direction from axial to radial due to the presence of an obstruction i.e. the heated surface. For axisymmetry jets the stagnation point exists at the central axis of the nozzle. This is the point where the jet comes to a complete stop before it is displaced by the incoming fluid. Almost always, the maximum

pressure in the system will be noticed here due to the dynamic contribution of the impinging fluid. In many literatures heat transfer coefficient and Nusselt number values at the stagnation point are considered as a good indicator of cooling process effectiveness [24].

The third region is a wall-jet zone where the dominant velocity component is radial and the boundary layer thickness increases monotonically as the fluid moves radially outward (see Figure 4). Some literatures further classify this zone as acceleration region and parallel-flow region. Whatever the case, the stream wise velocity increases in acceleration region to the value of incoming jet velocity with increasing distance.

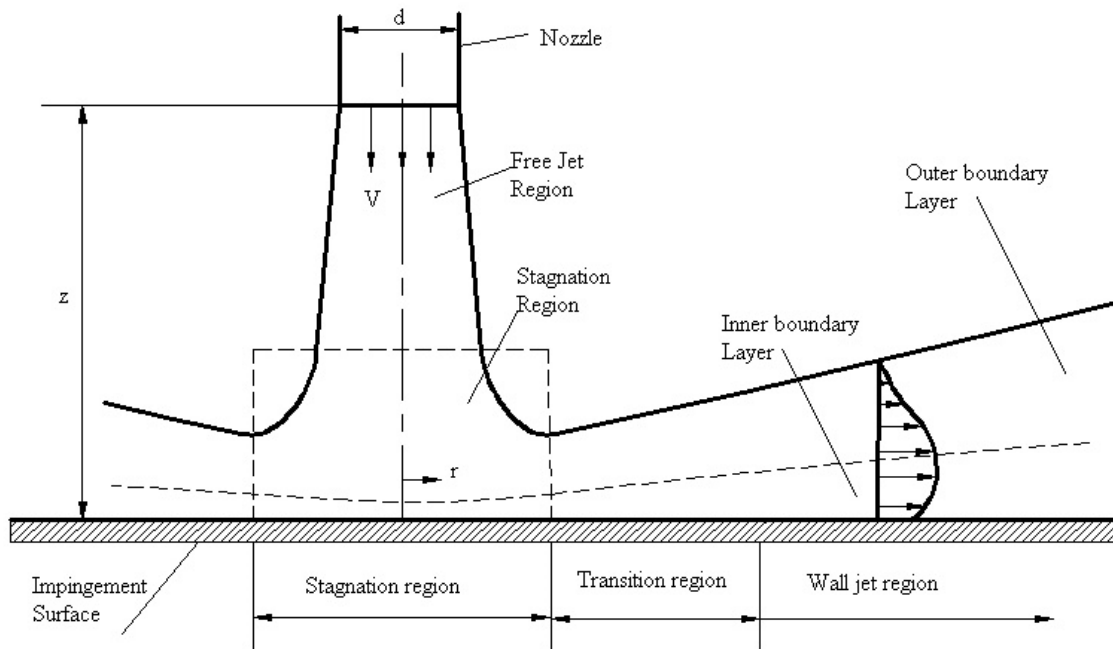


**Figure 4. Regions on the target surface due to an impinging circular jet [22]**

Thomson et al. described five main jet configurations in their literature reviews [25]. Figure 5 shows free-surface jets, plunging jets, submerged jets, confined jets, and wall jets. For plunging and submerged configurations with low jet velocity, large nozzle-to-surface spacing and/or large pool height the incoming fluid sometimes fail to penetrate and come in contact with the heated surface. As the jet exits the nozzle momentum exchange between the two miscible fluids makes it difficult for the jet to penetrate through the internal flow field.

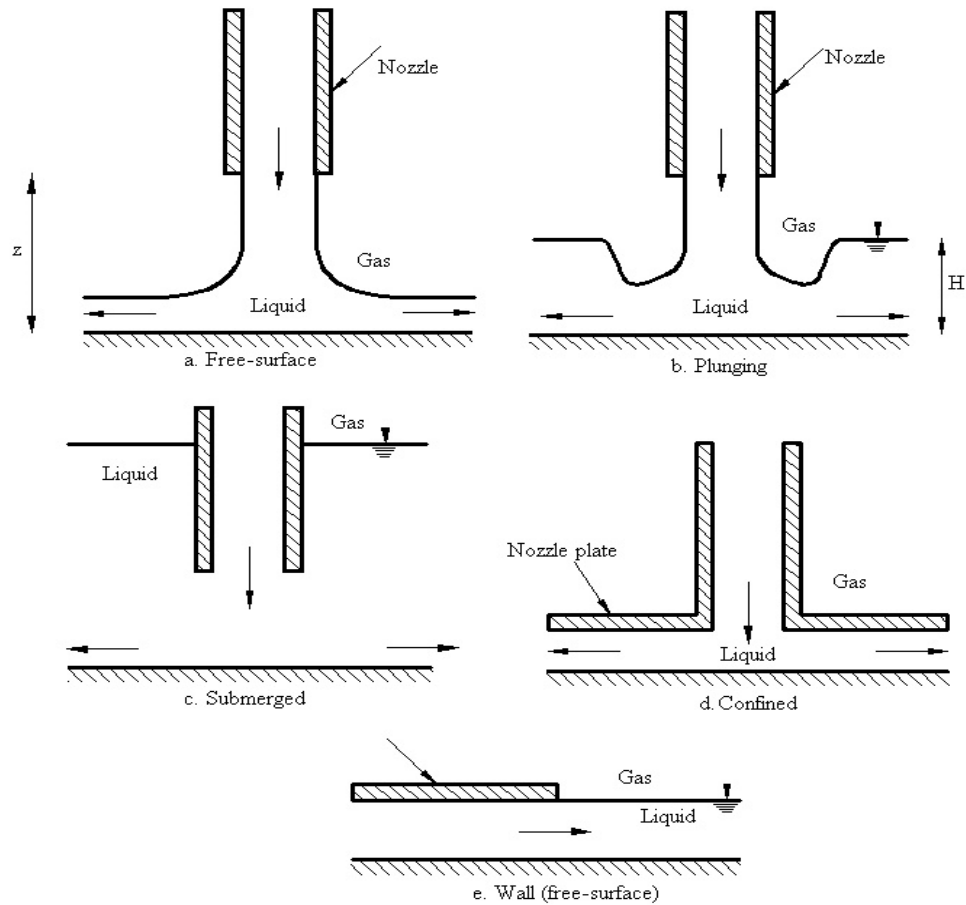


**Figure 5. Schematics of (a) Free surface (b) Plunging (c) Submerged (d) Confined and (e) Wall impingement configurations [26]**

## **2.8. Advantages and Disadvantages of Jet and Spray Cooling**

Selecting a cooling technique for a specific process involves a compromise on technical, cost and complexity of accompanying components and effectiveness of the method chosen. For example, sprays are more difficult to characterize than phase change mechanisms. The reason is other mechanisms, even jet impingement, can be easily developed using a characteristic length and velocity. However as the spray leaves the nozzle, liquid starts to breakup and form droplets with dissimilar diameters and velocities and trajectory directions become random. These and many more characteristics make choosing a scaling parameter for spray a lot more complex [27]. Nonetheless, based on previous studies several specific advantages and disadvantages on using spray cooling and jet impingement are noticed. So the designer has to be convinced to what extent he/she is willing to sacrifice in selecting either of the methods. Advantage and disadvantages of the two cooling methods are explicitly described by Bernardin et al. [9] and Collin et al. [28].

## **2.9. Droplet Dynamics**

For spray cooling, despite smaller residence time of liquid droplet on hot surface, the rate at which heat flux removed is much higher than nucleate boiling. Moreira et al. [29] and Jia et al. [30] show that each individual droplet splash, rebound, spread or sticks depending on the effects of surface tension, viscous force and inertia. Splashed and rebounded droplets reside on the surface for a snap of time but spread and stick droplets

form liquid film on the surface. Therefore the denser the spray the more complex the interaction of the droplets is going to be.

Apparently a rebounded and splashed droplet is in contact with the heated surface for quite a small time as a result it will not have ample time to exchange heat with the surface. However the study showed a single droplet analysis does not represent a spray cooling since spray cooling involves continuous undefined interaction of droplets with each other and with the surface. As shown in Figure 6, Bernardin showed that phase change starts after the droplet sticks and spreads.

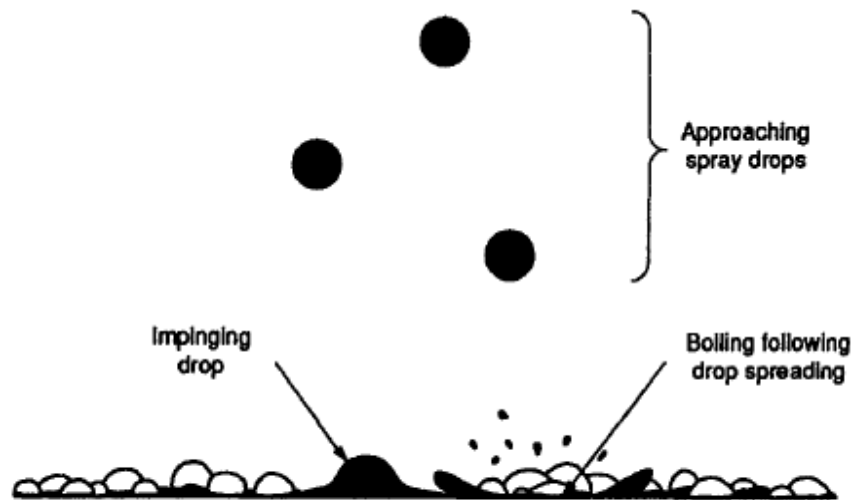


**Figure 6. Phase change in light sprays [27]**

For low velocity droplets and surface temperature of 150 – 360 °C Makino et al. also studied residence time of a droplet using a high-speed photography and reported that the droplet spreads outward into a thin film before phase change. A low droplet velocity



ensures little or no breakage of the droplet upon impingement. The reader is advised to refer to papers [31 - 37] for further understanding on droplet dynamics.

### **2.10. Droplet Sound**

Despite the fact that residence time of liquid on heated surface is lower for spray/jet cooling than pool boiling, impingement cooling is proven to be more effective in removing higher heat flux [38, 39]. Lloyd et al. studied quench cooling by impinging a 2 mm diameter water jet on to heated copper and brass test pieces of 94 mm diameter and 59 mm height located 45 mm below the test surface [37]. The heated test piece temperature ranged from 104 to 378 °C. They analyzed the vigorousness of jet breakdown to droplets and the associated sound generated as the jet hits the heated surface and nucleate boiling takes place using high-speed video camera and microphone. Finally they generated boiling sound to surface temperature relation which has a noisy-quiet-noisy-quiet pattern that helps to decide at what stage the cooling process occurs.

For surface temperature of 300°C and above, a kind of explosive pattern was noticed on the surface. This shows at lower temperature only heterogeneous nucleation boiling occurred and at higher temperatures a combination of homogeneous and heterogeneous nucleation may have occurred. In conclusion they argued for solid temperatures in the range from 250 to 300 °C the surface was subjected to repeating cycles of wet and dry and stable film boiling could not be confirmed which implied transition phase change may not always proceed in chaotic manner.

## **2.11. Factors Influencing Heat Transfer**

Design of a heat transfer component, enhancing cooling performance and using a technique for wide range of applications are highly dependent on addressing the parameters that influence the rate at which heat is removed. These attributes of heat removal designs are usually addressed in the majority of research without considering the effect of other factors. Many of the flow characteristics have compound affects on heat removal process and this makes the process more perplexing [4]. For example, erosion is a practical concern for a system with high-velocity jets (>5 m/s). High velocity impinging jets have a tendency to erode the heated surface on which they fall. This erosion in effect alters the surface finish of the target plate which also affects the heat transfer coefficient due to roughness. [For further explanation please see an interesting discussion by 40].

### **2.11.1. Confinement**

For a circular or rectangular nozzle of certain hydraulic diameter in confined water jet impingement, the flow is treated laminar if the Reynolds number is less than 2300 otherwise it is turbulent. Behnia et al. studied the effects of confinement and nozzle-exit attributes for axisymmetric jet impingement using a numerical turbulence model  $v^2-f$  [15]. After validating the numerical model they produced with experimental data they have studied the effect of different parameters on heat transfer coefficient. Fluid impinging in confined and unconfined settings for a wide range of Reynolds number values, Behnia et al. has shown how confinement leads to a reduction in average heat transfer rate while the local stagnation heat transfer coefficient is unchanged. They

also illustrated that confinement has little effect on heat transfer coefficient except at a very low nozzle to plate distance ( $H/D < 0.25$ ); however the nozzle characteristics strongly affect the heat transfer process especially around the stagnation region.

Colucci et al. in their experimental analysis concluded that local heat transfer coefficients or the dimensionless local Nusselt numbers for confined jets are more sensitive to Reynolds number and nozzle-to-plate spacing than unconfined jets [2]. Another experimental study on confined and submerged turbulent jet impingement is also done by Fitzgerald et al. [41] and San et al. [12] using laser-Doppler velocimetry. Fitzgerald et al. found out that for  $2 < H/d < 4$  the magnitude of the radial turbulence levels are not affected by a change in Reynolds number. San et al. concluded for  $H/d = 2$  that unconfined and confined impingements are proportional to 0.6375 power of Reynolds number alike. They also showed that jet diameter is a strong factor that affects the Nusselt number for diameter values less than 6 mm [12, 33 and 42].

### ***2.11.2. Nozzles and Jet-to-Target Spacing***

Three fourths of literatures written about the parameters that affect heat transfer process consider the effect of jet-to-target spacing; therefore any literature on enhancement can be referred. Katti et al. after series of experiments and analytical calculations, come to a conclusion that an increase in Reynolds number increases the heat transfer at all radial locations for a given  $H/D$  [22]. For a given Reynolds number, due to an increase in near wall turbulence intensities the stagnation point Nusselt number increases as  $H/D$  changes from 1 to 6. For decreasing  $H/D$  below 1 for lower jet-to-plate spacing Nusselt number increases because of flow acceleration.

### **2.11.3. Fluid Types**

Lin et al. carried out a spray cooling experiment in a closed loop using four different fluids as working medium [43]. They evacuated all gases from the system to a pressure below  $5 \times 10^{-6}$  Torr before filling up 38% of the internal volume [44]. Eight miniature nozzles placed 8.8mm away from the surface are used to generate a conical spray array ( average cone angle ranging from 35-50° with pressure drop from 0.69-3.10 bar) targeting a  $1 \times 2 \text{ cm}^2$  heated surface. The closed loop spray cooling can reach the critical heat flux levels up to  $90 \text{ W/cm}^2$  with pure FC-87,  $490 \text{ W/cm}^2$  with pure methanol and greater than  $500 \text{ W/cm}^2$  with pure water. They concluded that critical heat flux increases with an increase of the volumetric flux or pressure drop and non-condensable gases are found to affect the overall heat transfer adversely. However, the effect is highly significant only at lower heat flux than CHF due to non-condensable gases' higher thermal resistance to condensation. [10, 31, 15]

### **2.11.4. Nozzle Geometry, Angle, and Inclination**

Garimella conducted an experiment to determine the local heat transfer coefficient for axisymmetric normal FC-77 liquid jet impingement [18]. The result shows the heat transfer coefficients are the highest for very small nozzle aspect ratio of  $l/d < 1$  due to flow separation and reattachment in the nozzle. As the aspect ratio increases the coefficient sharply reduces, but it slowly increases as the aspect ratio increases further [18]. Following quite a number of experiments and looking at the results R.H. Chen said, “in order to achieve the highest feasible critical heat flux while using a minimum amount of water, it is important to select nozzles that produce a small droplet diameter with high

velocity” [38]. They concluded that, “dense sprays are not helpful for enhancing liquid usage efficiency while dilute spray increases the efficiency of liquid use.” In other words, a dilute jet spray with large velocity yields a higher efficiency.

Design of nozzles that would give the known stagnation Nusselt number trends is discussed extensively by Rahimi et al. [34]. The study focuses on heat transfer with under expanded jet impinges onto a heated surface where the surface interferes with the expansion process. The effects of normal and oblique shock waves at nozzle exit to bring back the flow to ambient pressure, supported by experimental data, suggested that the flow Nusselt number is a function not only of Reynolds number but also nozzle Mach number, and pressure ratios as well.

Peper et al. conducted an experiment that compares radial and inline jets with regard to heat transfer, wall pressure distribution and pressure loss [4]. To one’s surprise the result underline that radial jet nozzles with optimal flow exit angles of  $45^{\circ} - 60^{\circ}$  allow a high potential of heat/mass transfer increase for many purposes. Up to 60% and 50%, respectively, higher local and average heat transfer coefficients are possible compared with a standard circular inline jet of the same volumetric flow rate and the same average flow exit velocity. The lower impact force on the heated surface in using radial jets also favors its applicability for cooling stress-sensitive products [12]. Gulati et al. investigate the effects of nozzle shape specifically circular, square, and rectangular nozzles on local and average Nusselt number. Experiment assisted with infrared thermal imaging technique is performed for Reynolds number of 5,000–15,000 and  $H/d$  from 0.5–12. The result shows that average Nusselt numbers are insensitive to nozzle shapes [33].

A. Y. Tong examined the effects of Jet Reynolds number, jet impingement angle and jet inlet velocity profile in one paper. He observed that for inclined impingement the maximum Nusselt number location and the maximum pressure location shift upstream from the geometrical impingement spot which in effect influences the overall heat transfer rate. He also shows the heat transfer rate is highly affected by fluid inlet velocity magnitude and nature and Nusselt number also is directly proportional to the square root of Reynolds number [45].

### ***2.11.5. Nozzle Configurations and Outlet Design***

Lee et al. have studied the effect of nozzle outlet design on turbulent heat transfer improvement by using three different nozzle configurations. They found out that around the stagnation point a sharp-edge orifice jet yields a higher heat transfer rate than the others [46]. Whereas Baydar created jets between two parallel horizontal plates by piercing one of the plates and studied the effect of nozzle shape, Reynolds number and nozzle-to-plate spacing [42]. Chizhov et al. also have devised a predictor-corrector finite-difference scheme to study the impact of a very small scale compressible nitrogen liquid droplet (of the order less than 1 mm) at high velocity (100 m/s) on hot surface [25] and Pasandideh-Fard developed a numerical water droplet model impacting on a hot stainless steel surface [47].

Oliveira worked on residual stresses determination and distribution of the substrate as a result of the impingement pressure from the jet [48]. The result showed spray with controlled air pressure can give much wider fluid flow rate with a readily controlled range of operating pressure. However, the heat transfer rate lies between that

of air jet cooling and the liquid bath. O' Donovan and Murray examined the effect of impingement angle from 30° to 90° for a jet Reynolds number of 10,000 from 2 to 8 nozzle-to-plate spacing. The heat transfer distribution they obtain reveals the highest heat transfer takes place at the stagnation point [49].

Bhattacharya et al. estimated heat transfer in spray evaporative cooling as a multi-droplet array of liquid at low spray flux density by using analytical model and CFD simulation [50]. They have used a 4 mm thick steel strip as a heated surface and a critical droplet size of 70 μm for analysis. It is observed that smaller droplets may be capable of providing the increased cooling load of ultra fast cooling for thicker steel strips and critical droplet size decreases as steel strip thickness increases. In general, the smaller the droplet size the higher the cooling load to achieve for thicker strips. However, as drop size increases energy input for atomization is also increased significantly.

The attributes that fine droplets take more heat have made spray cooling the method of choice in many heat treating operations, especially those involving aluminum alloys. During solution heat treating, metallic alloy parts are first preheated to a temperature slightly below the melting point in order to dissolve the alloy solutes into the primary metal matrix (aluminum). The part is then rapidly quenched in order to freeze the solid microstructure attained during the preheating process. Finally, the part is reheated to some intermediate temperature to allow the hardening solutes to coalesce into sites which are finely and uniformly dispersed within the grains of the primary metal.

The finely dispersed solutes act as dislocation barriers, resisting deformations resulting from externally applied forces and resulting in a material with high strength and

hardness. Slow (poor) quenching may have disastrous consequences in heat treating, as it may result in a material with very poor strength and hardness. Therefore, the implementation of spray cooling in any heat treating operation demands a systematic methodology for predicting both the temporal and spatial variations of heat flux across the spray impact area. [16]

Spray cooling, sometimes known as mist/steam cooling, also has a vital application in keeping the workability and integrity of gas turbine blades. A typical medium scale gas turbine performs at about 30 bar. Therefore, a coolant at higher flow rate, about 20-30 times the normal Reynolds number value is required. Li et al. used water droplets less than  $10\mu\text{m}$  added to 1.3 bar steam and injected on a heated turbine blade. For a Reynolds number ranging from 7,500 to 22,500 and heat flux value of 3.3 to 13.4 kW/m<sup>2</sup> mist cooling is observed to enhance the heat transfer by 50-700% at the stagnation line [51, 52].

#### ***2.11.6. Dimensionless Parameters***

Whatever results found on an experimental analysis cannot be inferred to another application with different working medium unless an applicable scaling analysis is performed. Surface tension, inertial and viscous factors can be expressed using dimensionless parameters Weber and Reynolds numbers. Laplace and Capillary numbers to describe drop impact mechanisms.

Sensible heat required to heat the liquid up to its saturation temperature to the amount of heat needed to vaporize the liquid is scaled using Jacob number. As a definition, the Jacob number expresses the relative importance between the maximum



sensible heat absorbed by the liquid to the latent heat absorbed in accomplishing phase change. Sensible heat is associated with single-phase heat transfer, and the latent heat absorbed is associated with phase change, which makes Jacob number a two-phase heat transfer parameter. Influences of these parameters on heat transfer through spray impingement are discussed extensively by Panão et al. [53, 54] and Rittidech et al. [55] as they study effects of heck valves and aspect ratio on the overall heat transfer.

#### ***2.11.7. System Parameters***

In studying the effect of system parameters on phase change heat transfer for free-surface, circular jet has been investigated more extensively than all the other types of arrangements. Wolf et al. has studied effects of different parameters on heat flux. Some of the parameters are discussed below in Table 1 [26]. Single phase jet impingement has been studied through theoretical, experimental and numerical analyses for long. The studies make use of air or any liquid (especially refrigerants) as a working media. After carrying out many experiments and simulations non- dimensional empirical correlations have been proposed and the effects of many flow parameters were investigated. Elements that influence heat transfer process in general are listed as follows:

- Jet-to-plate spacing (this parameter affects the local heat transfer coefficient distribution) [41, 42, 2]
- Geometry of impingement substrate [56, 5, 7]
- Curvature of target plate [2]
- Roughness of the target plate [57, 49, 1, 20, 5, 7, 8]
- Reynolds number, dependent on jet velocity and diameter [41, 42, 2, 31]

**Table 1. Effect of system parameters on phase change heat transfer**

<b>JET TYPE</b>	<b>PARAMETER</b>	<b>EFFECT ON HEAT TRANSFER</b>	<b>COMMENT</b>
Free- Surface; Circular Jet and Planar Jets	Jet Velocity	No Effect	Heat Transfer depends only on wall superheat
	Subcooling	No detectable effect for a range of $T_{sub}(4-78\text{ }^{\circ}\text{C})$	However, it shows some effect near bubble incipience
	Fluid Property	Strongly depends on the type of fluid employed	Surface tension has an inverse relationship with Heat flux
	Nozzle/ Heater dimension	For fully developed Nucleate boiling, jet diameter & heater diameter has no Effect	For a range of heater-to-jet diameter ratio ( $14 < D/d < 54$ ) it has an effect
	Surface Orientation/ Impingement Angel	( $0 - 45^{\circ}$ ) No noticeable effect	-
	Nozzle-to-Surface Spacing	No effect for spacing $< 0.5d$	However, it is affected for larger spacing
Submerged, Confined and Plunging Jets	Jet Velocity	No Effect; Heat Transfer depends only on wall superheat	The fully developed boiling region for forced convection did not coincide with the extrapolated results for pool boiling
	Subcooling	No detectable effect for a range of $T_{sub}(4-78\text{ }^{\circ}\text{C})$	However, it shows some effect near bubble incipience
	Nozzle/ Heater dimension	For fully developed Nucleate boiling, jet diameter & heater diameter has no Effect	For a range of heater-to-jet diameter ratio ( $14 < D/d < 54$ ) it has an effect
	Nozzle-to-Surface Spacing	No effect for spacing $< 0.5d$	However, it is affected for larger spacing

In addition, other elements that influence heat transfer process are listed below:

- Mach number and, Prandtl number [31, 47]
- Jet confinement [42, 12, 15]
- Impingement orientation from the vertical and target plate inclination [58, 4, 45]
- Radial distance from stagnation point [39, 45]
- Nozzle inlet/exit geometry [2, 23, 34, 33, 37, 18, 46]
- Turbulence and turbulence intensity at nozzle exit [38]
- Spray characteristics [28, 29, 2]
- Fluid thermo-physical properties and dissolved gases [27, 44]

## **2.12. Literature Review Conclusion**

Bergles et al. commented on one of their reviews that “about 10% of the heat transfer literatures written these days focuses on cooling enhancement, and in average the *Journal of Heat Transfer* publication has over 20% of the papers dedicated to various areas of enhancement” [1]. However there is hardly any research done on enhancing the heat transfer rate by changing the profile of the impingement surface itself in macroscopic level. The overall goal of the present study was to show the dependency of heat transfer rate on the shape of an impingement surface and also determine the optimum shape of the heated surface that gives the best heat transfer rate.

## CHAPTER 3

### PROBLEM FORMULATION AND METHODOLOGY

#### 3.1. Jet Impingement without Phase Change

In response to specific objective one described in the first chapter, to determine shapes which maximize heat transport from heater surfaces using jet impingement cooling method, a problem description of optimizing the impingement shape is presented. Figure 7 shows a jet impinging on a heated flat surface model. Heat was input as a constant flux at the lower surface and a cooling fluid jet entered through a nozzle located at the top center. After impinging on the heated surface the fluid carrying the excess heat was allowed to exit the chamber through two exit ports. However unlike other confined jet impingement chambers the model used in the present study has side walls and the outlet was located at the top. Therefore the fluid could exit only at the periphery of the top surface, as shown schematically in Figure 7.

The flow in the control volume can be described by Navier-Stokes equations with appropriate boundary conditions as shown in equations 3.1 through equation 3.3. The problem description and equations have been solved using a CFD code commercially available from Fluent®, software which can solve the listed mass, momentum, and energy equations simultaneously. The solution to the momentum equations is a velocity flow field which gives a complete description of a particle position in time.

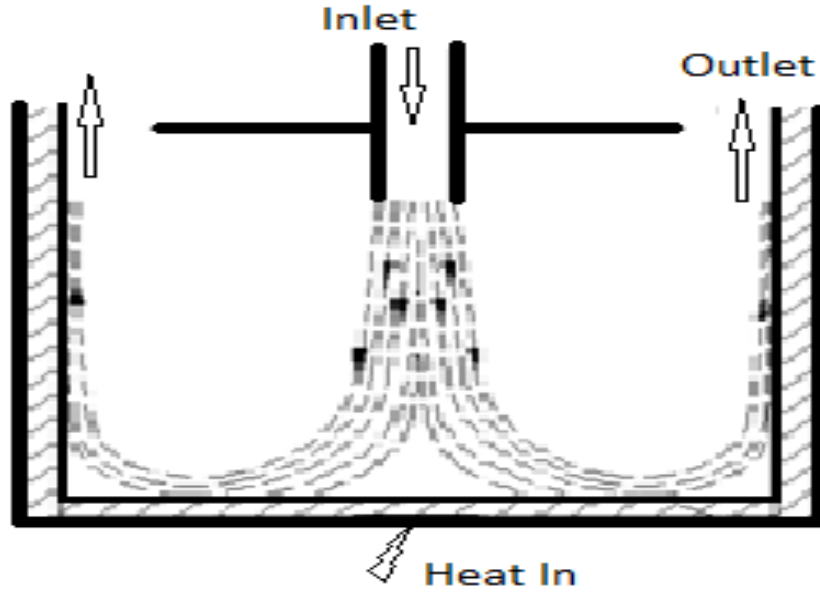


Figure 7. Simplified Heating Chamber Model

$$\frac{\partial \rho}{\partial t} + \sum_{n=i}^k \frac{\partial(\rho u_n)}{\partial x_n} = 0 \quad (3.1)$$

$$\frac{\partial(\rho u_i)}{\partial t} + \sum_{n=i}^k \frac{\partial(\rho u_i u_n)}{\partial x_n} = -\frac{\partial p}{\partial x_i} + \frac{1}{\text{Re}} \sum_{n=i}^k \left[ \frac{\partial \tau_{in}}{\partial x_n} \right] \quad (3.2)$$

$$\frac{\partial(T_i)}{\partial t} + \sum_{n=i}^k \frac{\partial(u_n T)}{\partial x_n} = \sum_{n=i}^k \left( -\frac{\partial(u_n p)}{\partial x_n} + \frac{1}{\text{Re}} \left[ \frac{\partial(u_n \tau_{in})}{\partial x_n} + \frac{\partial(u_n \tau_{jn})}{\partial x_n} + \frac{\partial(u_n \tau_{kn})}{\partial x_n} \right] \right) \quad (3.3)$$

Boundary conditions:

Inlet:  $y = 0$ ,  $u = 0$ , for the nozzle but  $u = u(x)$ , in the flow field and  $v = U$

Stagnation point  $y = h$ ,  $u = 0$ , and  $v = 0$

For cells other than the stagnation region:  $y = h$ ,  $u = u(x)$  and  $v = v(x)$

At the base:  $q = \text{heat flux input}$

Since no species transfer is expected in the analysis the species mass fraction convection term is set to zero. When the impingement shape is different from a flat surface the presence of wedge affects the flow and the N-S equation reduces to the well known Falkner-Skan equation for Newtonian flow [59]. The continuity equation stays the same but the momentum equation changes to equation 3.4

$$u \frac{\partial u}{\partial x} + v \frac{\partial v}{\partial x} = U_{\infty} \frac{dU_{\infty}}{dx} + \nu \frac{\partial^2 u}{\partial y^2} \quad (3.4)$$

where the free stream velocity in space is given by

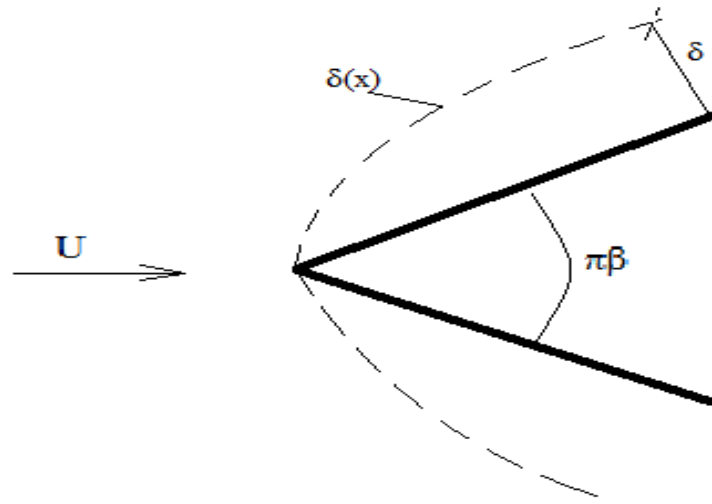
$$U_{\infty}(x) = U_{\infty} x^m \quad (3.5)$$

Figure 8 shows the boundary layer created as fluid flows over a wedge of angle  $\pi\beta$ . Majority of analysis done on Falkner-Skan flow of fluid over a wedge uses a half wedge angle measurement rather than the total angle. The current study also uses half angle measurement and whenever a wedge angle  $\alpha$  is mentioned it should be noted that it represents half of the overall wedge angle measurement,  $\pi\beta$ . When the wedge angle measurement changes from  $0^0$  to  $90^0$  the problem ranges from flow over a flat plate to impingement on a flat surface. Angular measurements larger than  $90^0$ , where the wedge shape changes to a concave grooved surface, are also studied.

Attaching the coordinate axis along the incline boundary conditions for a half wedge angle is given as:

$$y = 0, \quad u = 0, \quad \text{and} \quad v = 0,$$

$$\delta \rightarrow \infty, \quad u = U_{\infty}(x)$$



**Figure 8. Boundary layer on flow over a wedge**

Figure 9 shows preliminary data on numerical flow visualization in 3D chamber. The dynamics of particles with the impingement surface and away from the stagnation region is a complex process. However the fluid in the chamber has an axisymmetric flow field about the central axis. The axisymmetry nature of the flow across the center gives a basis for modeling a 2D simulation rather than the computationally expensive 3D model. Comparison on preliminary results shows 2D modeling is sufficient for the specific objectives required.

To simplify the complexity of the model each additional feature to the solver is introduced one at a time. First, a simple 2D rectangular model with a small inlet at the top and heat input at the bottom is considered as shown in Figure 7 earlier. The input parameters that describe the model are shown in Table 2. The foregoing 2D model was found to be computational less expensive in optimal shape search.

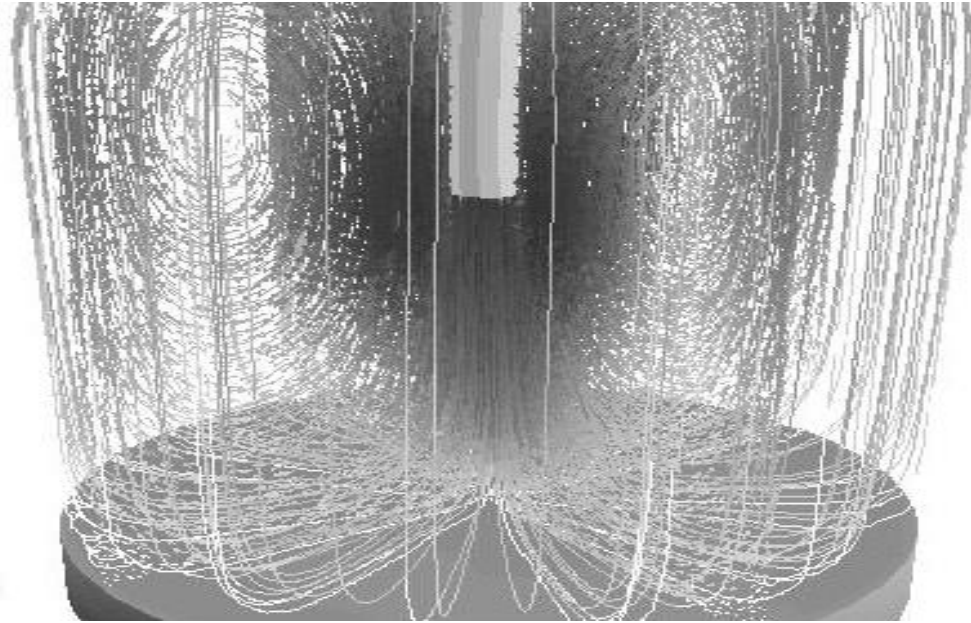


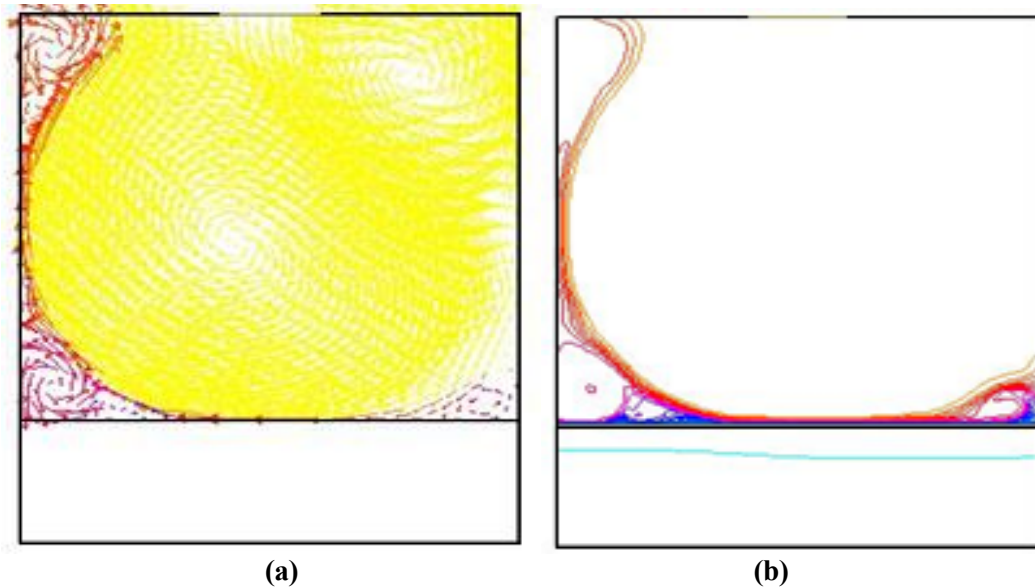
**Figure 9. 3D simulation of particle pathlines upon impingement**

**Table 2. Description of modeling parameters for jet impingement simulation**

<b>Property</b>	<b>Values</b>
Fluid Type	Air
Model Type	2D
Model size	0.1m diameter x 0.09m high
Nozzle diameter	0.01m
Heat Flux input	1 MW/m <sup>2</sup>
Impingement Velocity (Reynolds number)	5 m/s (Re=5000)
Exit condition	50% incoming fluid exit on either sides
Base plate material and thickness	Aluminum, 12.2 mm
Webber number	425.35
Nozzle-to-impingement surface distance, H/D	1.8 – 3.6



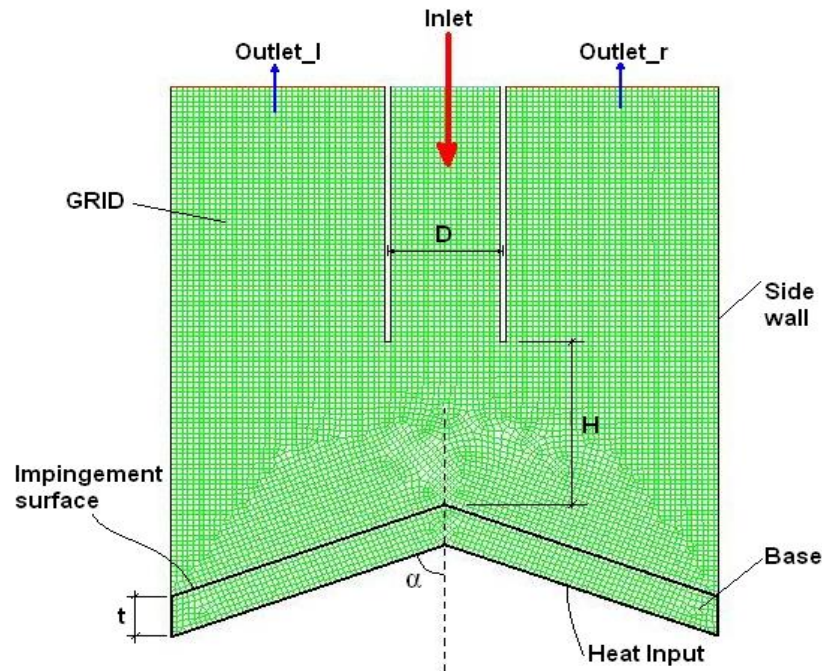
Figure 10, which were preliminary data, shows a velocity vector field and the corresponding temperature contour when jet inlet is far from the impingement wall. Looking at the preliminary simulation results, the injected fluid is unable to penetrate through the flow field of the control volume, as a result the flow swirl inside the chamber as a big vortex. This is not an effective way of cooling a high heat flux surface because there is a significant amount of flow separation at the corners and velocity drop throughout the chamber.



**Figure 10. Plot of (a) Velocity Vector and (b) Temperature contour of initial simulation model**

The preliminary data led to the final problem description as presented in Figure 11. Here the inlet to the chamber is extended further down up to about mid way of the control volume. Nozzle tip to surface distance is chosen based on the experimental setup

built. For simulations on the current study, depending on the profile of the impingement surface distance to nozzle diameter ratio,  $H/D$ , ranges from 1.8 to 3.6. Figure 11 explains important zones and boundaries generated using Gambit software.

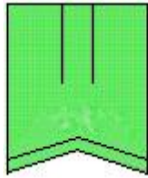
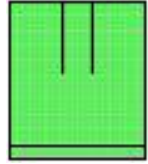
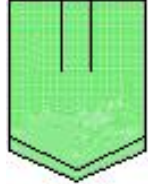


**Figure 11. Schematic of representative model used in simulation**

Table 3 shows the text matrix used in the study. A half wedge angle,  $\alpha$  is used as a way of comparison of the different models. For the sake of naming in this thesis, pointed wedges with half angle measurement less than  $90^\circ$  are called pointed or “A-type” wedges and those wedges with half angle measurements between  $90^\circ$  and  $180^\circ$  are called grooved or “V-type”. Four “A-type”, four “V- type” and a flat model are considered to study the effect of surface wedge angle on heat flux. The wedge angle cannot be lowered

or increased indefinitely due to flow separation noticed in the simulation while doing that. The flat impingement surface is taken as the benchmark for comparing the performance of the modified substrates.

**Table 3. Model half wedge angles**

Model Type		Model Name	Half Wedge Angle, $\alpha$
A-type		A0	70.2°
		A1	74.4°
		A2	78.7°
		A3	84.3°
Flat		Flat	90.0°
V-type		V4	98.0°
		V3	103.5°
		V2	109.0°
		V1	113.8°

### ***3.1.1. Single Phase Modeling Process***

Grid Generation: models are generated using CAD modeling software, Gambit. Each vertex is assigned with proper boundary conditions, and for information transfer between zones the fluid regime and the solid part are split one from the other. Due to the slant shape of the impingement surfaces a Quad-Pave type of meshing scheme is used. The number of nodes in the model depends on the overall surface area of the model.

Thus changing the shape of the surface changes the surface area of the model. However, this number is made as close as possible with identical grid spacing for all wedge types.

Setting up the solver and Input Parameters: for the search of an optimum impingement surface profile a Volume of Fraction (VOF) model is selected. VOF model is developed to solve problems like sloshing and jet breakup in steady or transient case. Once the problem is initialized the single phase jet impingement process is basically a liquid-on-liquid flow.

Solution from a steady-state solver makes sense only if the process is independent of the initial conditions and there are distinct inflow boundaries for the phases. For this part of the study, to determine heat flux rate and surface temperature a time dependent unsteady solver is used. However, for a given Reynolds number and constant heat flux value the system eventually reaches equilibrium. Thus a steady state solver is also used to compare the final results.

For air jet with 5 m/s exit velocity from a 0.01m diameter nozzle the Reynolds number is  $Re \approx 5000$ . This Reynolds number value implies the jet impingement simulation is a fully turbulent flow problem. Hence the two-equation RNG (renormalization group) K-epsilon viscous model was selected and all the model constants are kept at their default values.

### ***3.1.2. Gravity Effect on Jet Impingement***

In all types of impingement configurations gravity plays a very important role in changing the nozzle exit velocity ( $V_n$ ) to an impingement velocity ( $V_j$ ). If the impingement surface is facing upward the fluid exiting the nozzle accelerates to a higher

impingement velocity. Whereas for downward facing impingement surfaces the jet moves against gravity hence the fluid decelerates. The two velocities can be represented with equation 3.6.

$$V_j = (V_n^2 \pm 2gz)^{\frac{1}{2}} \quad (3.6)$$

It is obvious to see from the relationship that for large  $V_n$  or small impingement spacing,  $z$ , the two velocities become approximately the same. The centerline jet velocity has similar value as that of nozzle exit velocity for a good range of 5 to 8 nozzle diameter (Wolf [26]). Therefore impingement surface placed beyond this range has an impingement velocity lower than nozzle exit velocity. Many literatures surveyed in chapter 2 have made no distinction between the two velocity values so in the present study the impingement velocity is assumed to be exactly equal to nozzle exit velocity.

### 3.2. Phase Change

In response to specific objective two described in the first chapter, to model a two phase jet impingement process that incorporates phase change at the impingement substrate, multiphase model with extra source term was developed in the present study. For a problem involving more than one phase, solving the momentum equation and heat balance of a single phase is no longer sufficient. The model uses the N-S continuity equation where the sum of volume fraction of the two phases in a cell is always unity. The fluid properties are determined by a Mixture model as expressed in equations 3.7, where index  $m$  is for Mixture.

Continuity, momentum and energy equations for the mixture model are given respectively in equation 3.7 through equation 3.9.

$$\frac{\partial \rho_m}{\partial t} + \nabla \cdot (\rho_m \bar{u}_m) = \dot{m} \quad (3.7)$$

$$\frac{\partial (\rho_m u_m)}{\partial t} + \nabla \cdot (\rho_m u_m u_m) = -\nabla p + \frac{1}{\text{Re}} \nabla \tau_m + S_M \quad (3.8)$$

$$\frac{\partial}{\partial t} \sum_{k=p}^q (\alpha_k \rho_k E_k) + \nabla \cdot \sum_{k=p}^q \alpha_k \bar{u}_k (\rho_k E_m + p) = \nabla (k_{\text{eff}} \nabla T) + S_E \quad (3.9)$$

where:

$$\rho_m = \sum_{k=p}^q \alpha_k \rho_k \quad \mu_m = \sum_{k=p}^q \alpha_k \mu_k \quad \bar{u}_m = \frac{1}{\rho_m} \sum_{k=p}^q \alpha_k \rho_k \bar{u}_k$$

Effective conductivity  $k_{\text{eff}}$  is the combination of fluid conductivity and turbulent thermal conductivity. Energy content of each phase is expressed with  $E_k$ . The variable  $\alpha$  is volume fraction of each phase and number of phases in this study is two. The last terms in the energy, momentum and continuity equations are the source terms which need to be written using user defined function (UDF) code.

Mass, momentum and energy source contributions in a cell for phase “p” and “q” are given in equations 3.10 through equation 3.12, respectively. Where  $h_p$  is enthalpy of phase p with reference to formation enthalpy and  $h_p^f$  and  $h_q^f$  are formation enthalpies.

$$m_p = -m_{pq} \quad \text{and} \quad m_q = m_{pq} \quad (3.10)$$

$$m_p \vec{u}_p = -m_{pq} \vec{u}_p \quad \text{and} \quad m_q \vec{u}_q = m_{pq} \vec{u}_q \quad (3.11)$$

$$H_p = -m_{pq} (h_p) \quad \text{and} \quad H_q = m_{pq} (h_p + h_p^f - h_q^f) \quad (3.12)$$

CFD solver Fluent® does not have the capacity to simulate phase change process with its inbuilt commands. However, it gives access to its internal equations to introduce modification or add a source term. In order to model the phase change process a C based UDF code was written. Mass and momentum sources in Fluent® are defined per unit volume therefore in the UDF subroutines mass transfer was multiplied by the volume fraction of each phase present in the cell. The sign convention for a source terms is positive and a sink term is negative. Table 4 shows the main input parameters that describe the phase change model.

**Table 4. Description of modeling parameters for phase change simulation.**

Property	Values
Fluid Type	Water
Model description	Same dimension and specification as the first model
Heat Flux input	10 MW/m <sup>2</sup>
Impingement Velocity	V= 0 for pool boiling study V= 2m/s for phase change jet impingement
Exit condition	A pressure outlet and outflow.
Base plate material and thickness	Aluminum, 12.2 mm
Stockes number	0.0046

### ***3.2.1. Multiphase Modeling Process***

Grid Generation: a model similar to the one constructed in section 3.1 was used for the current study as well. In contrast, uneven grid size was defined in both horizontal

and vertical directions in such a way that the smallest cells were near the impingement surface. The process helps to effectively track the location where high parameter changes such as phase change occur. The grid spacing and number of nodes used in the model are presented in the grid independence study in section 3.3.

Preprocessing: Fluent® has a number of predefined simulation schemes in the package. The Mixture model was chosen because of the following reasons based on physics of the problem. Preliminary tests were carried out to determine the efficacy of the model chosen so as to get a converging and meaningful solution at the end. The second specific objective of the study was defined as a phase change process where water was taken as the primary working fluid.

Preliminary tests were performed using parametric studies that assist the decision process in choosing the best solver for the current problem. The benefit was that the right solver insures a stable and converging solution. The first factor checked was the loading parameter. Particulate (vapor) loading, expressed in equation 3.13, was used to determine dispersion of the second phase in the flow field [60]. To determine dispersion of the second phase the average distance between particles was calculated using the following equation as:

$$\frac{L}{d_d} = \left( \frac{\pi}{6} \frac{1 + \kappa}{\kappa} \right)^{1/3} \quad (3.13)$$

where  $\kappa = \frac{\beta}{\gamma}$ , the value of  $\beta$  and material density ratio  $\gamma$  are respectively,

$$\beta = \frac{(\alpha\rho)_d}{(\alpha\rho)_c} \quad \text{and} \quad \gamma = \frac{\rho_d}{\rho_c}$$



Material density ratio for the phase change flow field is  $\gamma = 5.54 \times 10^{-4}$  which is way below the demarcating range for gas–liquid flow region (0.001). At the start of the simulation the value of  $\beta$  is zero because initially there is no vapor inside the control volume. For a small value of  $\beta$ , applying limit, the right hand side reduces to 0.806, which is an intermediate loading factor. In addition, the Stokes number has to be determined to select the most appropriate model which ensures stability and rapid convergence rate. The Stokes number was calculated as shown in equation 3.14.

$$St = \frac{\tau_d}{t_s} = \frac{\text{Particle response time}}{\text{System response time}} \quad (3.14)$$

$$\text{where, } \tau_d = \frac{\rho_d d_d^2}{18\mu_c} \quad \text{and} \quad t_s = \frac{L_s}{V_s} = \frac{\text{Characteristic length of the system}}{\text{Characteristic velocity of the system}}$$

Taking vapor as dispersed fluid the particle response time of  $\tau_d = 9.191 \times 10^{-5}$  sec. and for jet impinging on the surface, system response time of  $t_s = 0.02$  sec gave a Stokes number of,  $St = 0.0046$  which is a value less than one,  $St \ll 1.0$ . The condition  $St \ll 1.0$  implies the particles closely follow the flow field hence the choice of the model is dictated by a smaller computational time, accuracy and model simplicity.

Treating the two phases as interpenetrating continua the Volume of Fraction (VOF) model was initially used. However the VOF scheme required longer computational time and would sometimes become unstable with an abrupt increase in flow Courant number. The preliminary tests resulted in the choice of the Mixture model because it was stable and gave fast convergence rate. Mixture model was designed to solve for flows with dispersed phase volume greater than 10% [60]. Fortunately the

Mixture model has less computational cost and is even much simpler than VOF model.

Table 5 shows the material properties applied in the two phase flow modeling.

Phase change is a time dependent process hence simulation stability and early convergence demands the use of unsteady solver with a smaller time step. The time step was chosen to be as small as possible to allow information to diffuse from cell to cell effectively. The appropriate time step size and number of iteration in per time step is determined.

**Table 5. Material properties of two phase flow fluids**

<b>Property</b>	<b>Liquid /Water</b>	<b>Vapor</b>
Density [kg/m <sup>3</sup> ]	1000	0.5542
Viscosity [kg/m-s]	1.003x10 <sup>-3</sup>	1.34x10 <sup>-5</sup>
Thermal conductivity [w/m-K]	0.6	0.0261
Specific Heat, Cp [J/kg-K]	4182	2014
Molecular Weight [kg/kgmol]	18.0152	18.01534
Reference Temperature [K]	372	372

As described in Table 6, the sub-time step value of 0.57 is the minimum value that should be used to get information pass from cell to cell and insures convergence. A sub-time step value of 20, which is much larger than 0.57, was used for the iteration which means within each time step a fixed time stepping solver iterates 20 times to find convergence. The iteration was carried out even if the simulation did not converge

within the specified number of sub-time step because before the total number of time step ends the solution eventually did converge.

**Table 6. Minimum time step determination technique**

Step	Variable	Relationship	Value
1	Locate minimum grid size, $\Delta x$	Around impingement surface	$\Delta x=0.0224\text{m}$
2	Maximum flow velocity, $V_{\max}$	Exit of the nozzle	$V_{\max}=5.1 \text{ m/s}$
3	Frequency, $f$	$\frac{\Delta x}{V_{\max}} = \frac{0.0224}{5.1}$	0.0044
4	Sub-step size, $\Delta t_s$	$\frac{f}{\text{Courant no.}} = \frac{0.0044}{0.25}$	0.0176
5	Number of Sub-time steps	$\frac{\Delta t}{\Delta t_s} = \frac{0.01}{0.0176}$	0.5700

In selecting the material for the primary and secondary phases the general recommendation by the software developers was followed. The carrier continuous fluid – water - was set as the primary phase and the dispersed fluid – vapor - was set as secondary phase. In doing so, the Mixture model gives the option to specify the particle diameter for the secondary phase. Based on literatures the generally accepted vapor bubble detachment diameter value ranges from  $1.5 \times 10^{-6}$  to  $2 \times 10^{-4}$  m [61, 14]. The present study used a bubble diameter of  $2 \times 10^{-5}$  m.

The simulations were carried out assuming the impinged fluid exits to the atmosphere. Thus the operating pressure was set to an atmospheric pressure of 101325 Pascal. The operating pressure of the system was assigned at some reference pressure

location inside the model. Since Fluent recommends setting the location close to the lighter fluid the reference pressure location is set at close proximity to the heated surface. The location of this point differs from model to model therefore the right value is assigned after locating the grid node close to the stagnation point.

User Defined Function UDF: jet impingement phase change requires a pre-defined UDF subroutine in order to accommodate mass and energy transport. The objective is to use a single equation to solve the energy and momentum conservation equations of the two-phases and the portion of mass transfer in phase change. Conservation of Energy equation for a domain can be written in enthalpy (total heat content) form as equation 3.15.

$$\frac{DH}{Dt} = k\nabla^2 T \quad (3.15)$$

Expanding the substantial derivative gives:

$$\frac{\partial H}{\partial t} + u \frac{\partial H}{\partial x} + v \frac{\partial H}{\partial y} = k \left( \frac{\partial^2 T}{\partial x^2} + \frac{\partial^2 T}{\partial y^2} \right) \quad (3.16)$$

Basically change in enthalpy  $\Delta H$  is more meaningful in thermodynamic calculation than the total enthalpy value, H of the fluid. The total energy transfer through a process is equal to the sum of the internal energy content of the system  $\Delta U$  and work done by the system  $\Delta(PV)$  as in equation 3.17. However the system does not do any work to the surrounding; therefore the work done term  $\Delta(PV)$  is zero.

$$\Delta H = \Delta U + \Delta(PV) \quad (3.17)$$

In heating a liquid, energy transport in phase change takes place in form of sensible and latent heat. Sensible heat is responsible for the amount of energy absorbed

by a system as its bulk temperature increases up to its saturation temperature without phase change. As the temperature of the fluid reaches its saturation temperature, phase change takes place releasing huge amount of energy as latent heat of vaporization  $h_{fg}$ .

$$\Delta H = m(C_p dT + h_{fg}) \quad (3.18)$$

Energy equation is basically a volumetric equation; thus the above equation can be rewritten as equation 3.19. The two expressions on the right hand side of equation 3.19 are the ones responsible for sensible and latent heat transfers respectively. Change in enthalpy can be expanded further taking temperature as intermediate variable using chain rule. This shows the process is a function of temperature (See the derivation below.)

$$\Delta H = \rho C_p dT + \rho h_{fg} \quad (3.19)$$

$$\frac{\partial H}{\partial t} = \frac{\partial H}{\partial T} \times \frac{\partial T}{\partial t} \quad (3.20)$$

similarly,

$$\frac{\partial H}{\partial x} = \frac{\partial H}{\partial T} \times \frac{\partial T}{\partial x} \quad \text{and} \quad \frac{\partial H}{\partial y} = \frac{\partial H}{\partial T} \times \frac{\partial T}{\partial y} \quad (3.21)$$

However  $\partial H / \partial T = \rho C_p$  for sensible heat, i.e. slope of the two inclined lines in Figure 12 and for the discontinuous part (sudden jump)  $\partial H = \rho h_{fg}$  which is the latent heat value. In phase change process from liquid to vapor, for example, the heat content of the vapor phase will be increased by a magnitude of the latent heat of vaporization, as clearly described in Figure 12. Therefore, the energy content of the new phase is given by equation 3.22. The first terms in the bracket at the left hand side of equation 3.22 is usually approximated by  $m$  and reduces the equation to equation 3.23. However, the total

mass of a phase in the domain is calculated from the contribution of each cell's volume fraction  $\alpha$  containing that phase. Mathematically it is given in equation 3.24.

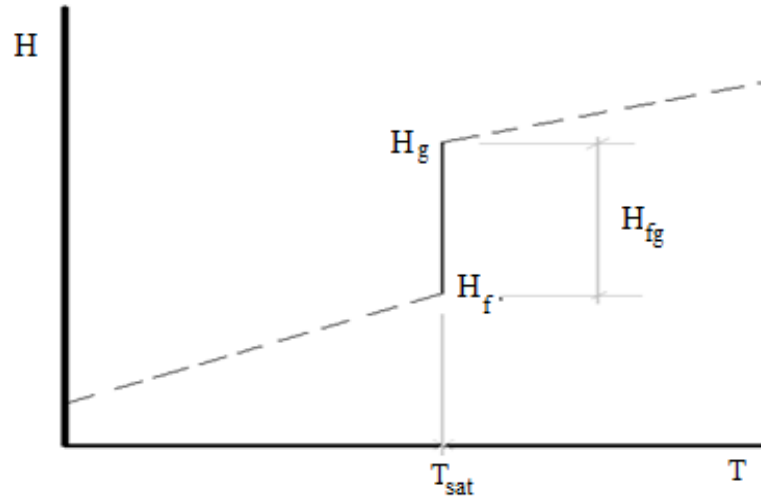


Figure 12. Phase change line on enthalpy–temperature graph

$$(m + \Delta m)C_p dT_v = \Delta m h_{fg} = \Delta m C_p T_{sat} \quad (3.22)$$

$$m(T_{sat} - T) = \Delta m T_{sat} \quad (3.23)$$

$$m = \sum \rho \alpha_v \quad (3.24)$$

Finally, the mass transfer in each cell becomes:

$$\Delta m = \frac{\rho \alpha_v (T_{sat} - T)}{T_{sat}} \quad (3.25)$$

The UDF code was written to solve for this expression in every cell where the temperature of the cell exceeds saturation temperature. The corresponding energy

transfer through phase change is simply the product of the mass transport by latent heat of vaporization.

$$E = \Delta m \cdot h_{fg} \quad (3.26)$$

UDF macros is used to solve for the source terms where the input parameters were local phase type, condition criterion of phase change, magnitude of change in the source equation, and cell identification number. The macros function was defined to operate on every cell; therefore, the developed UDF reads individual cell temperature, density, and volume fraction then pass the values to the solver to evaluate the mass transfer magnitude. The source term for energy was also written exactly in the same approach except the mass transport term is finally multiplied by the latent heat value.

Substituting these into the general enthalpy equation gives a temperature dependent energy equation with a subscript  $i$ , for the region in consideration. Thus to effectively solve this problem the relation is solved for the three different temperature zones jointly as shown below.

$$\left(\rho C_p + \frac{\rho h_{fg}}{T_{sat}}\right)_i \frac{\partial T}{\partial t} + u \left(\rho C_p + \frac{\rho h_{fg}}{T_{sat}}\right)_i \frac{\partial T}{\partial x} + v \left(\rho C_p + \frac{\rho h_{fg}}{T_{sat}}\right)_i \frac{\partial T}{\partial y} = k_i \left(\frac{\partial^2 T}{\partial x^2} + \frac{\partial^2 T}{\partial y^2}\right) \quad (3.27)$$

The three regions are:

- Pure liquid region:  $\mathbf{T} < \mathbf{T}_{sat}$  :

$$\left(\rho C_p\right)_l \frac{\partial T}{\partial t} + u \left(\rho C_p\right)_l \frac{\partial T}{\partial x} + v \left(\rho C_p\right)_l \frac{\partial T}{\partial y} = k_l \left(\frac{\partial^2 T}{\partial x^2} + \frac{\partial^2 T}{\partial y^2}\right) \quad (3.28)$$

- Interface boundary or Stefan condition [62]  $\mathbf{T} = \mathbf{T}_{sat}$  :

$$\left(\frac{\rho h_{fg}}{T_{sat}}\right) \frac{\partial T}{\partial t} + u \left(\frac{\rho h_{fg}}{T_{sat}}\right) \frac{\partial T}{\partial x} + v \left(\frac{\rho h_{fg}}{T_{sat}}\right) \frac{\partial T}{\partial y} = k \left(\frac{\partial^2 T}{\partial x^2} + \frac{\partial^2 T}{\partial y^2}\right) \quad (3.29)$$

- Pure vapor region:  $\mathbf{T} > \mathbf{T}_{sat}$  :

$$(\rho C_p)_v \frac{\partial T}{\partial t} + u(\rho C_p)_v \frac{\partial T}{\partial x} + v(\rho C_p)_v \frac{\partial T}{\partial y} = k_v \left( \frac{\partial^2 T}{\partial x^2} + \frac{\partial^2 T}{\partial y^2} \right) \quad (3.30)$$

In the liquid zone:

$$T_l(x, y, t) \Big|_{x=0} = T_b < T_{sat}; \quad t > 0$$

$$C_l \rho_l \frac{\partial T_l}{\partial t} = k_l \frac{\partial^2 T_l}{\partial x^2}; \quad t > 0 \text{ and } 0 < X(t)$$
(3.31)

In the vapor region:

$$T_v(x, y, t) \Big|_{t=0} = T_o; \quad T_v(x, y, t) \Big|_{x \rightarrow \infty} = T_o;$$

$$C_v \rho_v \frac{\partial T_v}{\partial t} + C_v \rho_v u \frac{\partial T_v}{\partial x} = k_v \frac{\partial^2 T_v}{\partial x^2}; \quad t > 0 \text{ and } X(t) < x < \infty$$
(3.32)

At the boundary,  $x = X(t)$ :

$$T_l = T_v = T_{sat}; \quad t > 0 \text{ and } 0 < X(t)$$

$$k_l \frac{\partial T_l}{\partial x} - k_v \frac{\partial^2 T_v}{\partial x^2} = \{h_{fg} \rho_l + (C_v \rho_v - C_l \rho_l) T_{sat}\} \frac{dX}{dt}$$
(3.33)

The outlet of phase change simulation domain was set to pressure outlet boundary condition. Since flow reversal was observed during the preliminary tests at the exit of the control volume back flow volume fraction is set for the liquid phase alone. In the phase change simulation, the detaching bubble was assumed not to return once it leaves the control volume therefore only liquid phase back flow volume fraction is set as unity. Table 7 summarizes the boundary conditions that are assigned in each phases, primary phase is the carrier fluid and secondary phase is the dispersed fluid.



**Table 7. Boundary conditions available for a multiphase model**

<b>B.C. Type</b>	<b>Primary phase</b>	<b>Secondary phase</b>	<b>Mixture</b>
Velocity inlet	None	Volume fraction	Velocity magnitude
Pressure outlet	None	Volume fraction	Back flow P and T
Outflow	None	None	Flow rate weighting
Wall	None	None	Heat Flux and No slip
Fluid	Mass source	Mass source	Energy source

The back flow temperature was also set as the temperature of the primary phase at the outlet. Momentum and volume of fraction problems are discretized with second order up-wind methods for better precision. For phase change, the discretization technique had a strong effect on the results. First order upwind discretization gave a quicker but unrealistic bubble shapes which did not interact with each other, specifically no coalescence or splitting. Whereas bubbles formed in second order upwind discretization were more realistic in shape and dynamics.

For the grid generated with quad mesh pressure is discretized scheme of PRESTO and pressure velocity coupling techniques of SIMPLEC were used. However, it was noted that the solution became more stable and robust when the under-relaxation factors for all variables were from their default values. The input variables are summarized at the end of this chapter.

Specific initial conditions were set for different sectors of the domain by over writing the starting conditions. Velocity inlet was used to initialize the velocity flow field

and the temperature field was initialized by custom field function. Double precision solver was used for the simulations. Many of the convergence monitors are set to  $10^{-6}$  and even further lowered for variables other than the energy solver because iterations do not converge completely due to round-off accuracy in the vicinity of the convergence criteria.

### **3.2.2. Gravity Effect on Phase Change**

Gravity effect for a phase change simulation is quite significant because the light weight fluid lift off because of buoyancy. Therefore gravitational effects were included in the simulations by assigning  $-9.81 \text{ m/s}^2$  in the Y direction. The operating density parameter was also turned on and taken as the lighter phase in the simulation, which is vapor phase with density value of  $0.5442 \text{ kg/m}^3$ . For a model that is significantly affected by natural convection, where vapor raises due to buoyancy, Boussinesq approximation is used for a fast convergence. The operating temperature for Boussinesq parameters is set to 372K, which is almost the saturated water temperature value.

Table 8 gives a summary of the parameters used in the model development. Based on the model type used, either for the first specific objective simulation or for the second objective, the appropriate parameter that should be used in setting up and initializing the solver is tabulated. For turbulence model, the default parameters were used whereas for coupling solver the relaxation parameters were tuned as the simulation go on so that the problem converge fast. The main boundary conditions for the solver are also given at the last row of Table 8.

**Table 8. Input parameters for modeling**

<b>Property</b>	<b>Parameters</b>
Solver	<ul style="list-style-type: none"><li>• Pressure based 2D Steady and Unsteady solvers</li><li>• Implicit Formulation</li><li>• Superficial Velocity, Absolute Velocity Formulation</li><li>• Cell-Based Gradient</li></ul>
Reference Conditions	<ul style="list-style-type: none"><li>• 101325Pa Reference Pressure Located near the heater</li><li>• <math>-9.81 \text{ m/s}^2</math> gravitational acceleration only in Y</li><li>• Op. Temp.= 299.8 K for air jet and 372K for phase change</li><li>• Vapor density was (<math>0.5442 \text{ kg/m}^3</math>) taken as operating density</li></ul>
Turbulence Modeling	<ul style="list-style-type: none"><li>• Two equation RNG K-epsilon model</li><li>• Thermal effect enhanced near-wall treatment</li><li>• Default modeling constants</li></ul>
Solver Controller	<ul style="list-style-type: none"><li>• For air jet impingement model Flow, Turbulence and Energy equations are solved together using SIMPLE coupling solver</li><li>• For phase change model Flow, Volume Fraction, Slip Velocity, Turbulence and Energy equations are solved together using SIMPLER coupling</li><li>• Skewness Correction = 0</li></ul>
Under-Relaxation Factors	For the applicable solver: <ul style="list-style-type: none"><li>• Pressure = 0.2</li><li>• Density = 0.5</li><li>• Body Forces = 0.5</li><li>• Momentum = 0.3</li><li>• Slip Velocity = 0.1</li><li>• Volume Fraction = 0.4</li><li>• Turbulent Kinetic Energy = 0.5</li><li>• Turbulent Dissipation Rate = 0.5</li><li>• Turbulent Viscosity = 0.5</li><li>• Energy = 0.5</li></ul>

**Table 8. (Cont.)**

<b>Property</b>	<b>Parameters</b>
Discretization	For air jet impingement simulation <ul style="list-style-type: none"> <li>• Pressure = PRESTO!</li> <li>• Momentum = Second Order Upwind</li> <li>• Volume Fraction = QUICK</li> <li>• Energy = Second Order Upwind</li> </ul> For phase change simulation <ul style="list-style-type: none"> <li>• Pressure = PRESTO!</li> <li>• Momentum = Second Order Upwind</li> <li>• Volume Fraction = QUICK</li> <li>• Energy = Second Order Upwind</li> </ul>
Boundary Conditions	For air jet simulation <ul style="list-style-type: none"> <li>• Heat in = a constant heat flux of <math>0.1\text{MW/m}^2</math></li> <li>• Inlet Velcotiy = 2m/s</li> <li>• Exit = outflow</li> </ul> For phase change simulation <ul style="list-style-type: none"> <li>• Heat in = a constant heat flux of <math>1\text{MW/m}^2</math></li> <li>• Liquid Inlet Velcotiy = 0 (pool boiling)</li> <li>• Liquid Inlet Velcotiy = 2m/s (phase changejet impingement)</li> <li>• Exit = pressure outlet (pool boiling)</li> <li>• Exit = outflow (phase changejet impingement)</li> </ul>

### 3.3. Grid Independence Study

Grid independence study is one important step that should be performed before considering any simulation output as a valid result. The grid independence study is carried out to make sure the results obtained from Fluent® are not affected by grid spacing and the number of nodes chosen. Sometimes truncation and round off errors affect a result so severely. For this reason a varying property such as static temperature is

used for monitoring grid dependency. The different impingement surface models then run for the same real time simulation with three different grid spacing values.

Table 9 shows the maximum temperature of impingement surface for 5 second real time simulation of the different models. The models were meshed with three types of grid spacing which gave a slightly different node numbers in the domain. As tabulated on Table 9 altering the grid spacing from 0.0005m to 0.002m doesn't have any effect on the result, therefore a grid spacing of 0.001m (1mm) somewhere at the middle of the aforementioned spacing was selected for all simulations. Residual plot of a simulation is also another convergence indicator. Depending on the solver type used, the residual monitoring tool shows the convergence history of different properties. Figure 13 shows a successful convergence history of continuity, momentum, energy and turbulence equations of the model which took about 1,700 iterations.

**Table 9. Grid independence study maximum temperature taken as the variable**

Model Type	Grid spacing, $\delta$ (m) and Maximum Temperature, T (K)					
	$\delta = 0.0005$	T	$\delta = 0.001$	T	$\delta = 0.002$	T
A Type wedge	40810 nodes	358	10390 nodes	358	2830 nodes	358
Flat Surface	43616 nodes	354	11108 nodes	354	3035 nodes	354
V-Shape Substrate	47681 nodes	362	12126 nodes	362	3307 nodes	362

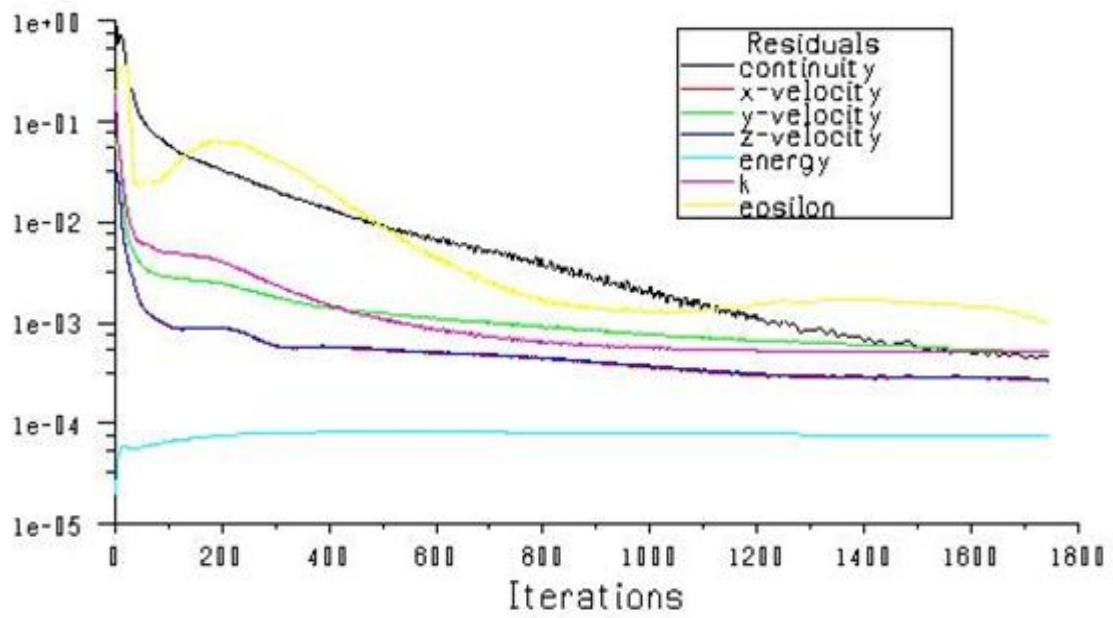


Figure 13. Plot of residuals

## CHAPTER 4

### RESULTS

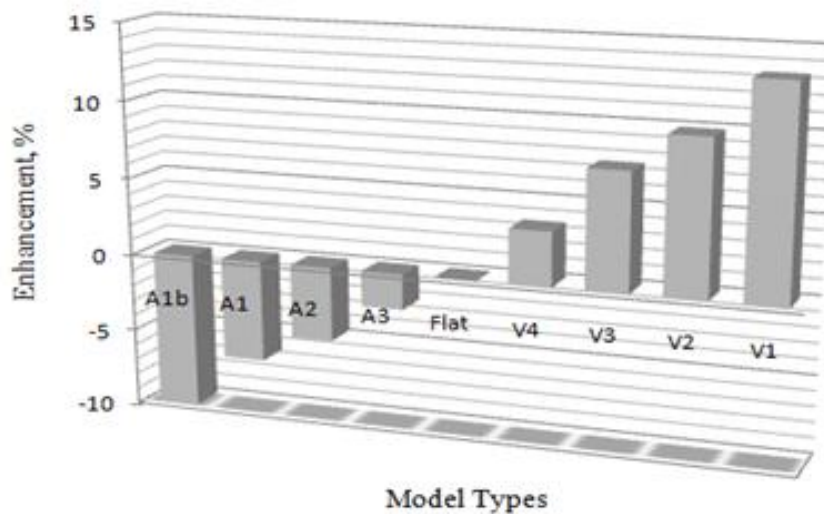
#### 4.1. Results of Optimum Shape Search

Table 10 summarizes surface heat flux distribution, maximum temperature in the model, and overall heat transfer enhancement obtained by modifying the impingement surface for 10 second real time simulation. For the problem described in section 3.1 applying the solving methodologies discussed in Chapter 3 these results are found using post processor tools in Fluent.

**Table 10. Summary of heat flux enhancement in changing the wedge angle**

Shape	Wedge Angle, [deg]	Max Temp [k]	Heat Flux [W/m <sup>2</sup> ]	Enhancement %
A1b	70.2	360	1257.1	-9.986
A1	74.4	358	1305.4	-6.528
A2	78.7	356	1330.3	-4.745
A3	84.3	355	1364.9	-2.267
Flat	90.0	354	1396.6	0.000
V4	98.0	355	1445.2	3.483
V3	103.5	357	1501.4	7.507
V2	109.0	359	1533.9	9.834
V1	113.8	362	1583.0	13.350

Figure 14 shows the heat transfer enhancement values of the different model types studied and percentage enhancement is depicted in a bar chart. The bar chart shows that V1-type model increases the heat transfer rate by 13.35% than flat impingement surface. The enhancement translates in an additional  $186.4 \text{ W/m}^2$  heat flux removed by modifying the flat impingement surface to the V1-type from a flat surface.

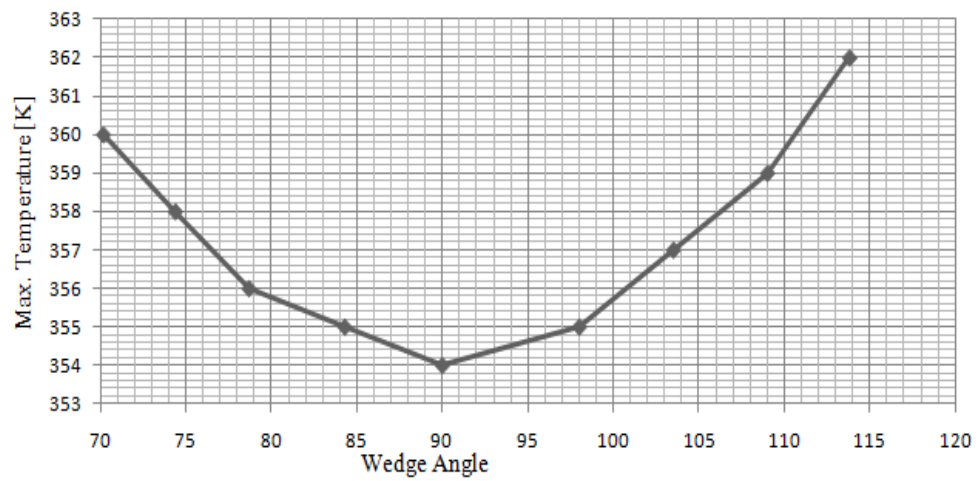


**Figure 14. Bar chart of enhancement for different models**

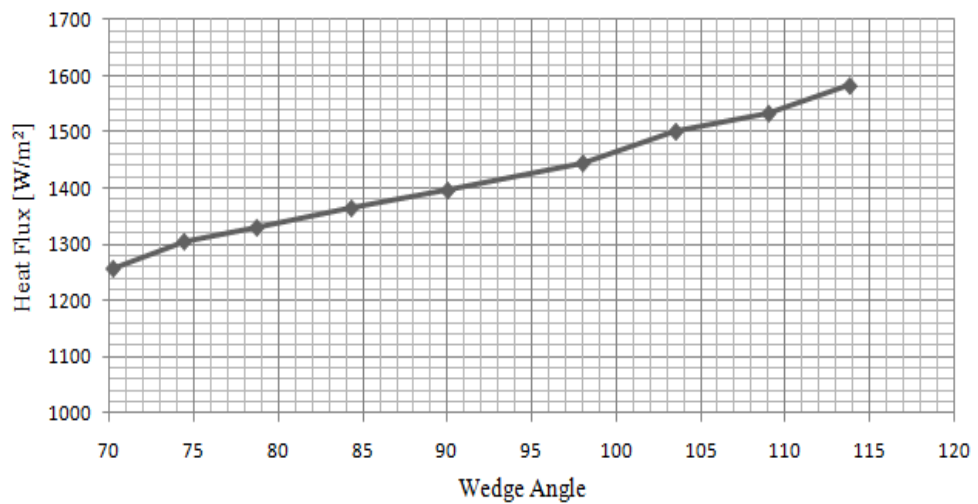
Figure 15 compares the maximum surface temperature of the models and average heat flux values as a function of wedge angle. From Figure 15(a) it can be concluded that although the flat model insures the lowest surface temperature, yet the model does not give a significant temperature drop when compared to other models. The corresponding average surface heat flux data shown in Figure 15(b) illustrates that the average surface heat flux increases in a nearly linear fashion as a function wedge angle. A flat



impingement surface is indicated by 90 degree wedge angle while models with angles less 90 degrees are indicated by A-type models which are found to have a less effective heat transfer rate than a flat impingement surface. Those models called V-type are found to have a better heat transfer rate than a flat impingement surface.



(a)



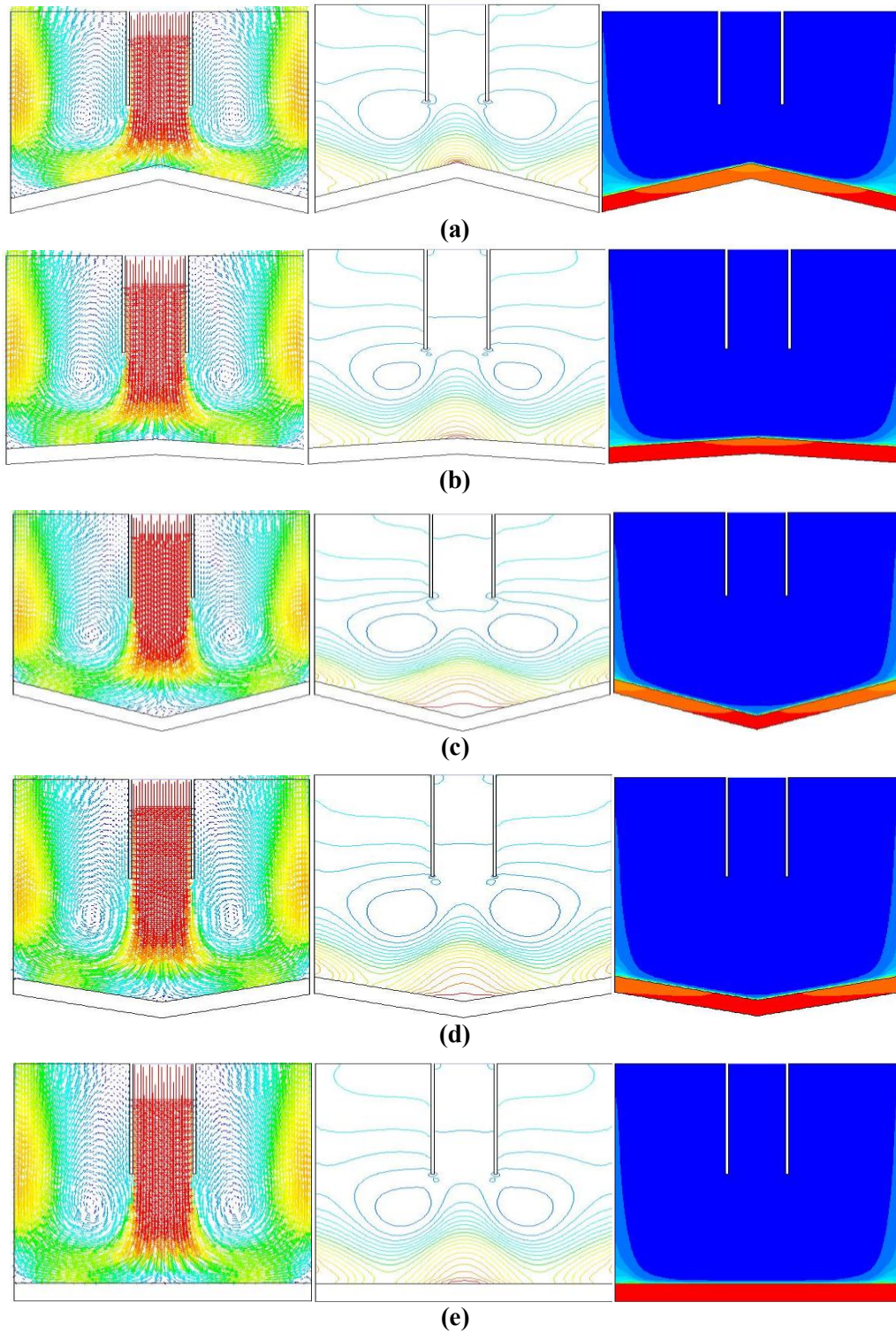
(b)

**Figure 15. Plot of surface (a) Temperature and (b) Heat Flux versus Wedge Angles**

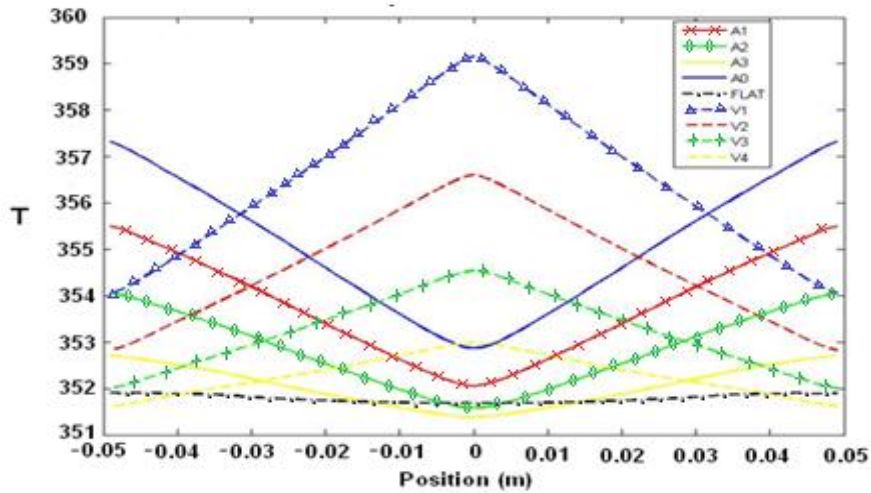
The results indicate that impingement surface shape modifications do have a significant effect on the overall heat transfer. The next task was to search for an optimum shape that would give a better performance than V1-type surface. The search for the optimum impingement shape was motivated by realizing that the flow field parameters have an effect on the heat transfer rate as shown in Figure 16. The figure shows a series of velocity, pressure and temperature plots of some of the different models used.

As the Figure 16 indicates there are significant flow separations at the corners of the A-type models. More specifically, the lower the deviation of the wedge angle from  $90^\circ$  the higher the flow separation in the corners. The difficulty of flow from reaching to the corner surfaces results in a lower convective heat transfer coefficient at that location which leads to a higher surface temperature. The flow separation is determined by inspecting the velocity vector plots and stream function contours.

In the flow separation corners, fluid particles circulate independent of the main flow at the corner which results in a reduction in heat transfer rate. For the V-type models, apart from the stagnation region, the flow streams stay in contact with much of the surface. The higher the wedge angle the smaller the flow separations noticed at the corners and the lower the surface temperature in those corners. The comparison can be understood by plotting surface temperature distributions versus position as shown in Figure 17.



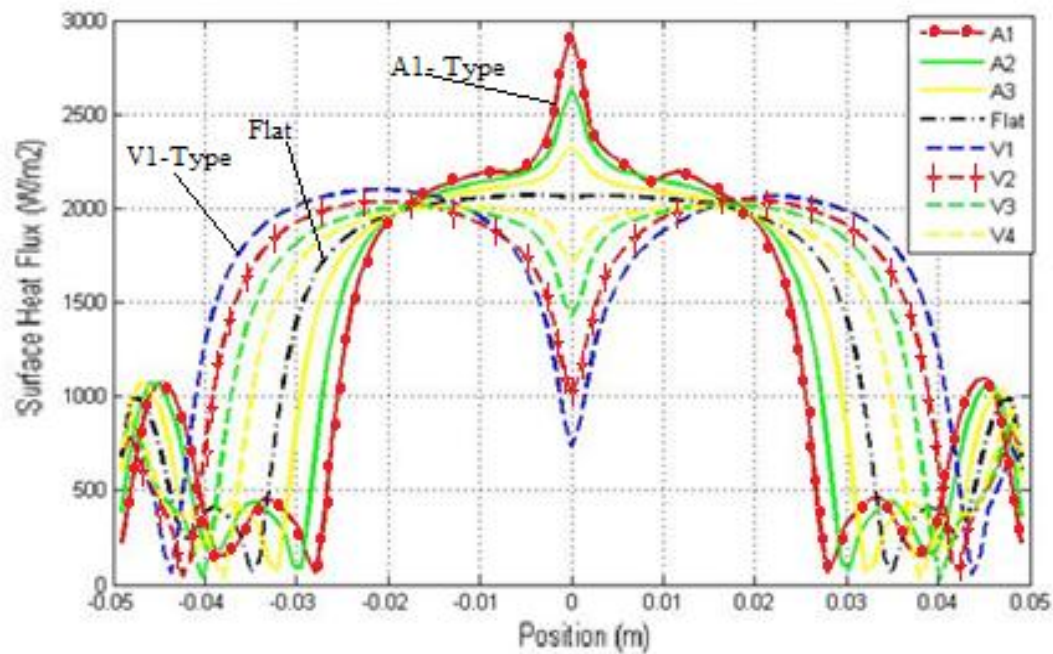
**Figure 16. Velocity vector, pressure contour and static temperature plots of (a and b) A-type model, (c and d) V-type model, and (e) flat surface model at 10 sececond time elapse**



**Figure 17. Surface temperature profile comparison of models after 10 second real time simulation elapse**

Figure 17 shows surface temperature distribution after 10 seconds time elapse for the different models considered. The data shows that both A-type and V-type models result in a higher temperature than the flat surface model. In addition the temperature difference between all the models is not larger than 8°C.

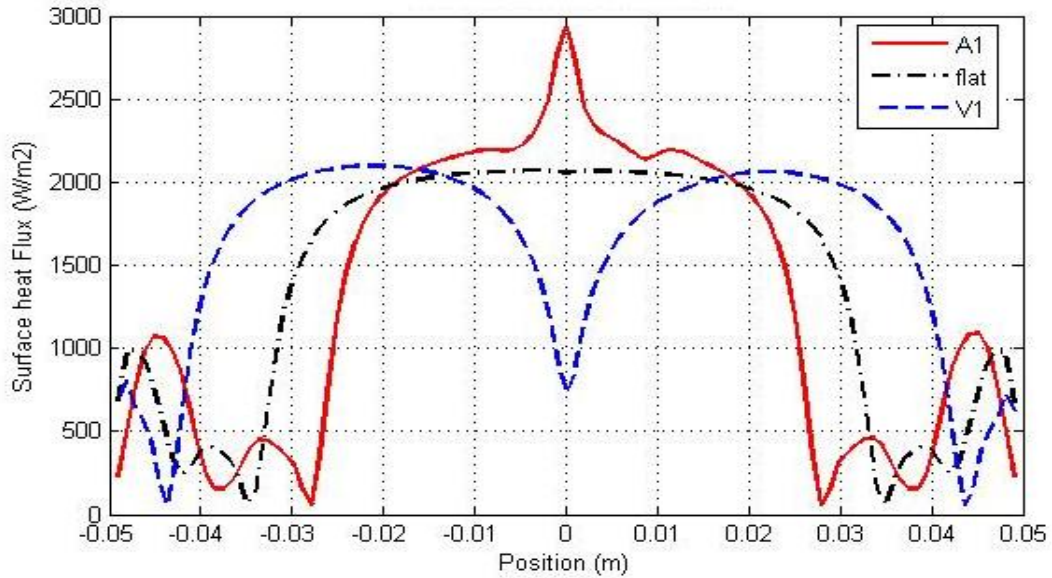
The second comparison involves surface heat flux profile at the impingement surface of different models used in the study shown in Figure 18. Figure 18 presents the local surface heat transfer data along the heated surface. Recall that A-type models are in general inefficient in their overall performance as shown in Figure 14. A1-type model however exhibits the maximum heat flux around the stagnation region ( $-0.015 < x < 0.015$ ). As the fluid start turning from axial to radial direction, V1-shape substrate becomes much more effective in terms of surface heat flux. Flat impingement surface lies in between and gives a uniform surface heat flux for the widest range.



**Figure 18. Heat Flux comparison of models analyzed at 10 second time elapse**

The foregoing results led to the realization that combining the two profiles which had the highest regional performance could result in a single profile which has a better heat transfer performance than the individual contributor. Figure 19 shows the model with local maximum surface heat flux where at the stagnation region the A-type model (A1) exhibits a better performance than the other models but away from the stagnation region the V-shape substrate (V1) has a better heat flux. Therefore, the new impingement model was derived using A1-type profile at the stagnation zone and V-type shape for the rest.

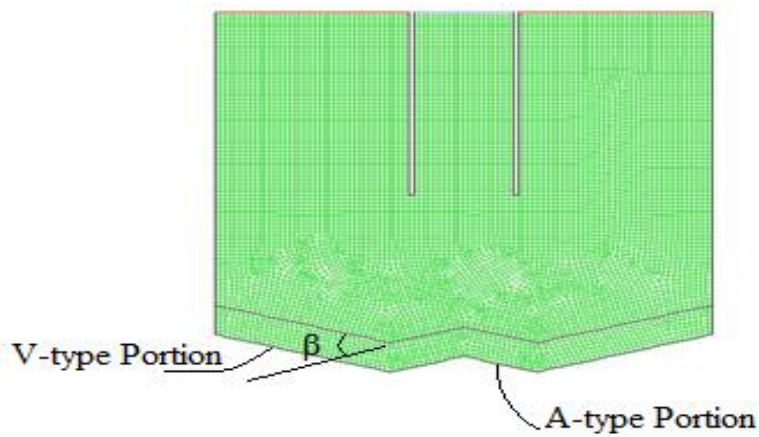




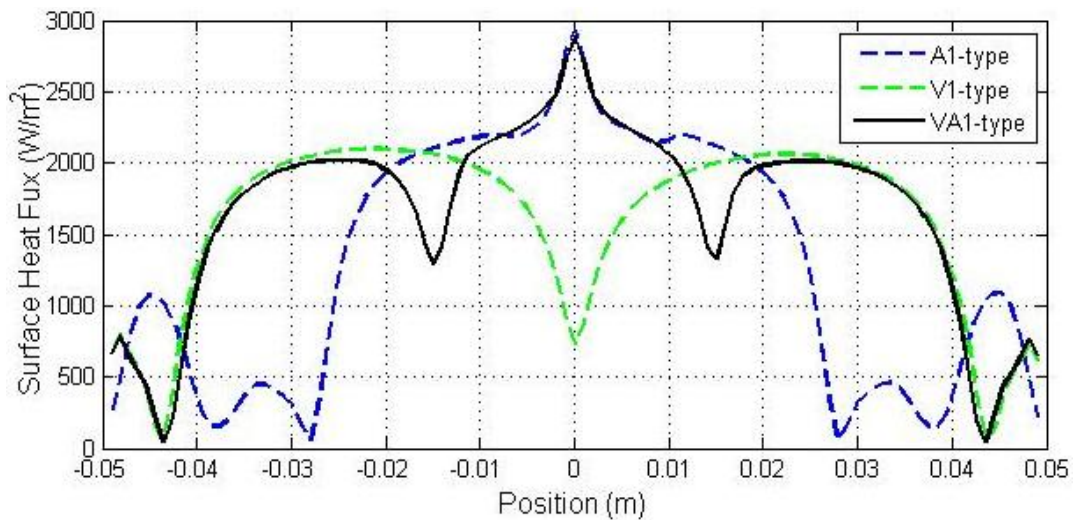
**Figure 19. Surface heat flux comparison of Modified shapes with flat surface**

Figure 20 shows a schematic of the new developed VA-type model. The transition angle from the A-type to the V-type shape is given by  $\beta$ . Four different models are constructed by changing the intermediate angle. Subsequently similar simulations with the same initial and boundary conditions as the A-type and V-type models were performed on these models. The results are compared in similar fashion on the basis of surface heat flux values as shown in Figure 21. Comparison of surface heat flux is shown in Figure 21. The heat flux distribution shows that the newly modified shape incorporates the benefit of the two shapes which yields a better performance than the original models. Around the stagnation region the new model follows the performance of that of the A1-type and when the fluid moves to the V-type region it follows the original

V-type model performance. However in the transition between the two regions there is a considerable performance drop. This performance reduction is due to flow separation taking place at the junction point. The new model has the highest heat removing capacity than the previous modifications.



**Figure 20. VA-type mode**



**Figure 21. Heat flux comparison with the new model**

Table 11 summarizes the data from the simulation where the maximum temperatures of the models are in a comparable range whereas the average heat flux is improved as depicted in Figure 22. The heat flux comparison in Figure 22, shows that VA3 model gives a superior heat transfer performance with an enhancement up to 20% when compared to the flat surface which is another 5.67% additional enhancement to the V1-type model. The optimum impingement shape search results in VA3-type model, which is composed of the regional high performing A1-type and V1-type models.

**Table 11. Comparison heat flux and overall enhancement of VA type model with the high performance A-type and V-type models**

Shape	Original Models	Max. Temp. [k]	Heat Flux [W/m <sup>2</sup> ]	Enhancement%
A1	-	358	1305.359	-6.531
V1	-	362	1583.032	13.352
VA_FLAT	A1 and Flat	355	1461.557	4.654
VA2	A1 and V2	358	1528.247	9.430
VA1	A1 and V3	357	1606.391	15.027
VA3	A1 and V1	359	1671.206	19.666

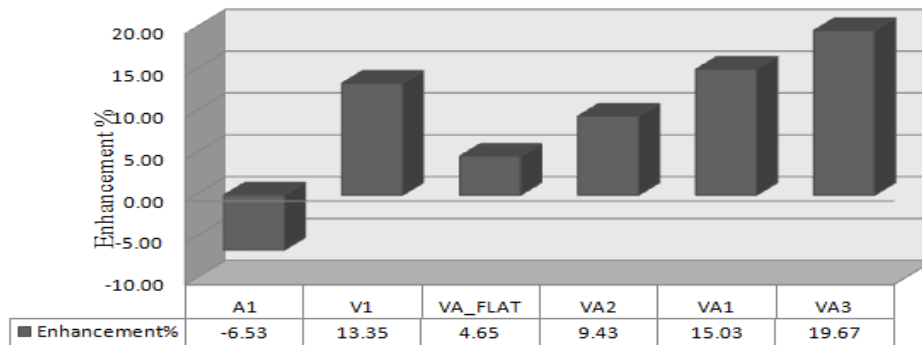


**Figure 22. Heat Flux Comparison of the newVA-type models**



Figure 23 presents the velocity vector, static pressure, and temperature fields of VA-type models . The figure shows that as the inclination of the V-type model increase the effectiveness of the shape increases. However, at the junction of the two model types there exist a flow separation which leads to a drastic drop in effectiveness.

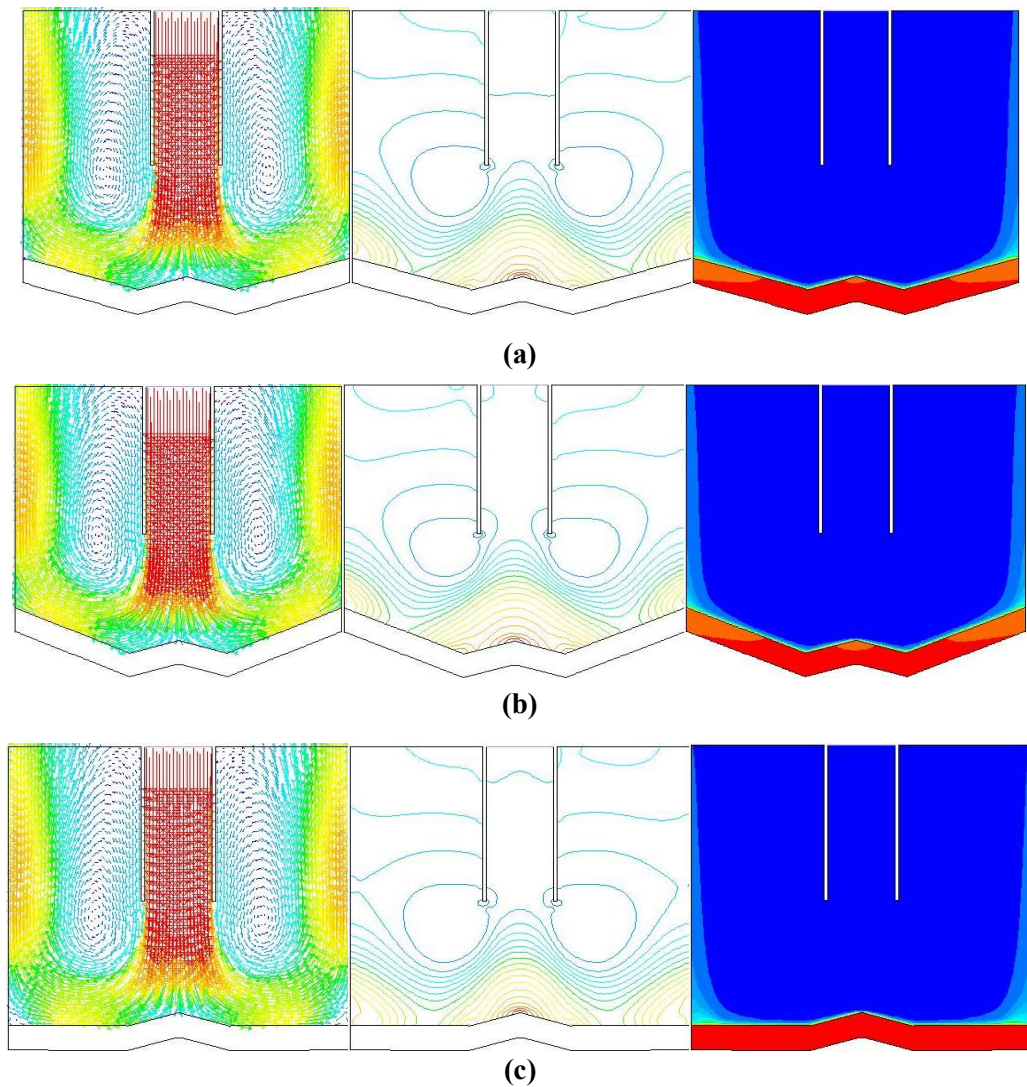


**Figure 23. Plot of velocity, pressure and temperature for (a) VA2-type (b) VA1-type and (c) VA-Flat models**

## 4.2. Results of Phase Change Jet Impingement

The task was to apply phase change on the last model generated (VA3 model) and study jet impingement heat transfer incorporating phase change process as described in the second specific objective. As explained in chapter 3, Fluent can not model a phase change process without a UDF code. Therefore, a UDF code that handles phase change process was written and compiled as described in chapter 3. The resulting code was run until bubble formation, coalesce and detachment on the heated surface is confirmed. Thus before applying a water jet with inlet velocity of 5 m/s (and 2 m/s for some analysis) the phase change CFD code is first tested using pool boiling simulation where the UDF code ensures phase change when the local conditions determined by temperature exceeds saturation temperature and condenses back when the temperature drops.

Two phase flow convergence history of Volume Fraction of Vapor and Area Weighted Surface Nusselt Number plots shown in Figure 24 and Figure 25, respectively. These plots were used to monitor the convergence history as flow time advances and to identify the instance bubble is created and lifted up. A sudden drop of vapor volume fraction at the surface indicates bubble detachment; for example, at 4 sec and 10.15 sec.

Figure 26 through Figure 28 show comparison of Surface Temperature, Heat Flux, and Surface Nusselt number distributions at different real time simulations, respectively using the phase change Model. The surface Temperature distribution in Figure 26 shows that the impingement surface temperature for phase change heat transfer increases with increasing time until it becomes steady (above  $T=550\text{K}$ ).

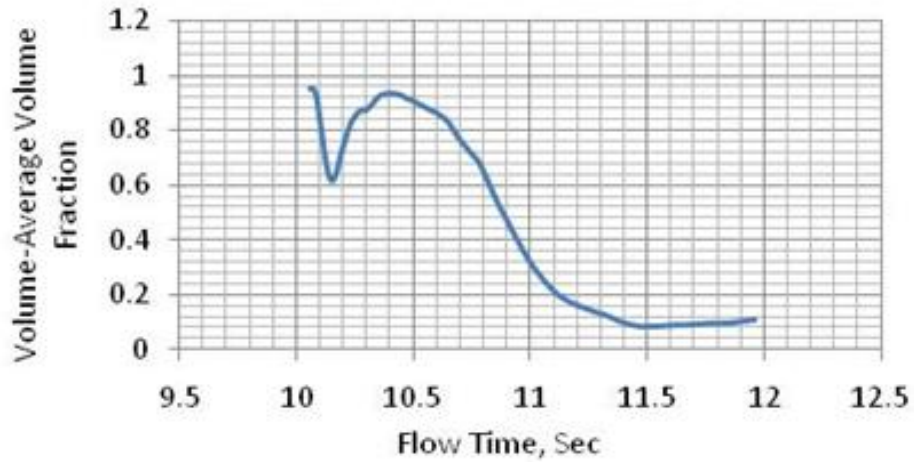


**Figure 24. Convergence history of Volume-Average Volume fraction of vapor**

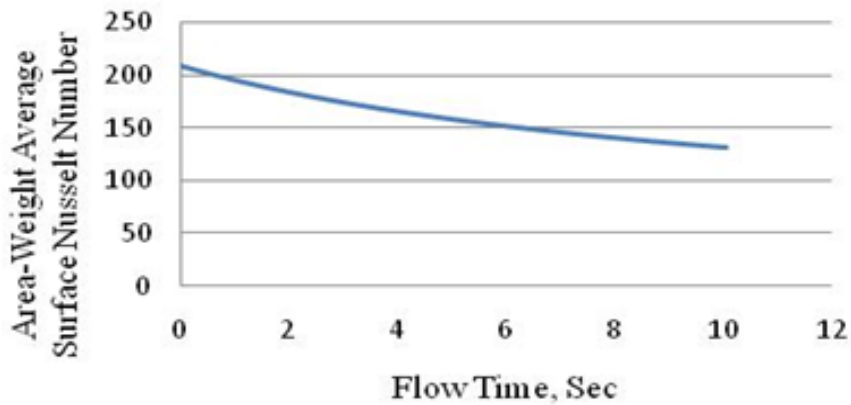


**Figure 25. Convergence history of Area-Weighted Average Surface Nusselt Number**

Conversely for jet impingement the surface temperature stays more or less the same throughout the process (around  $T=425K$ ). Figure 27 and Figure 28 shows jet impingement model with phase change has a higher heat transfer rate than pool boiling process, as expected from the physics of the problem.

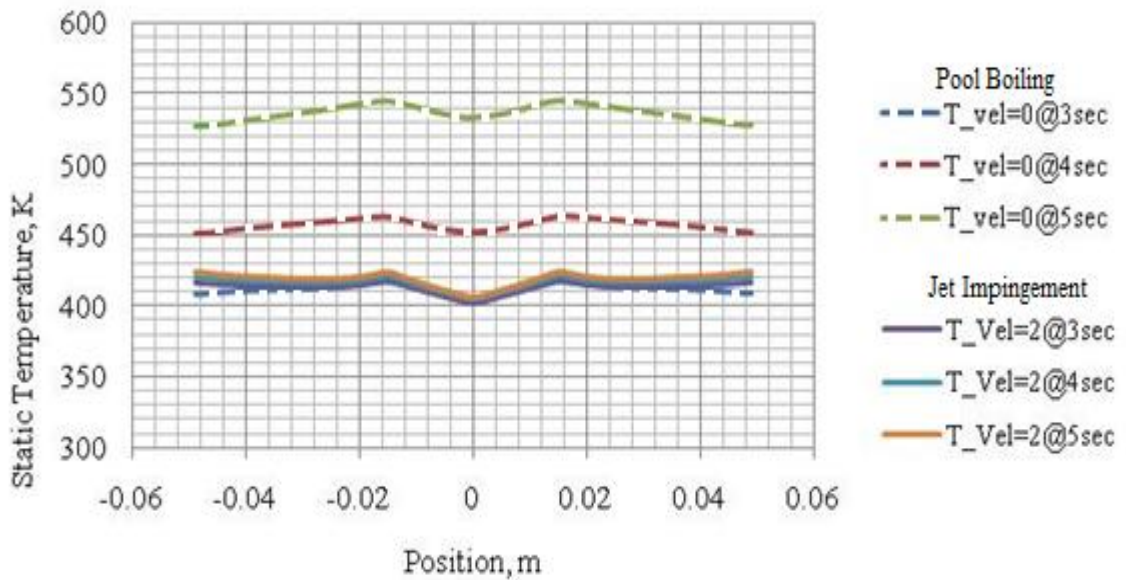


Figure 26. Temperature comparison for phase change models with and without jet impingement

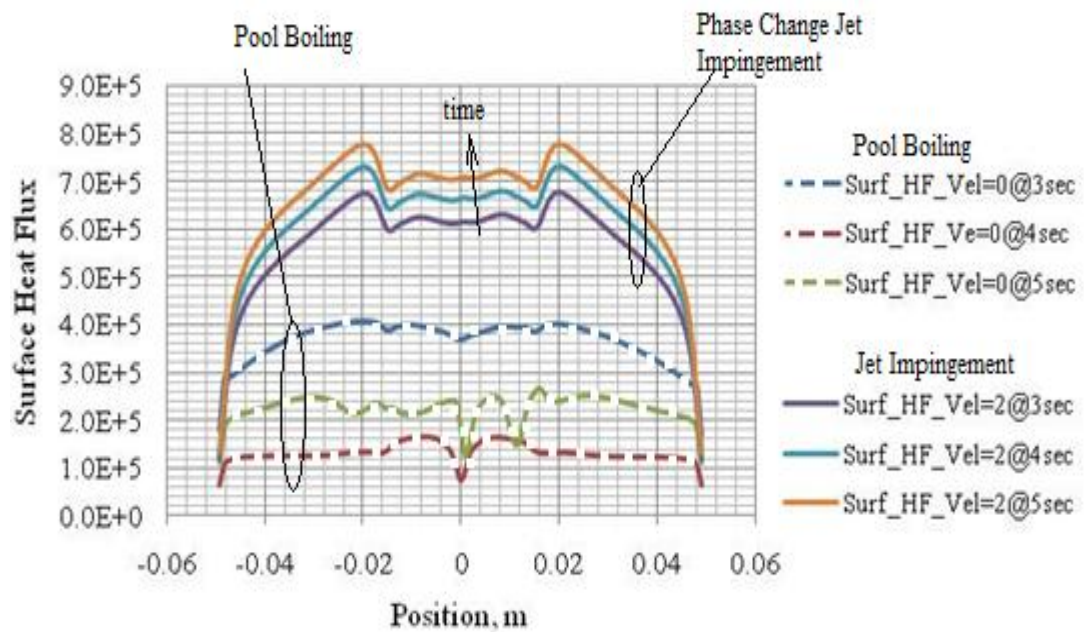
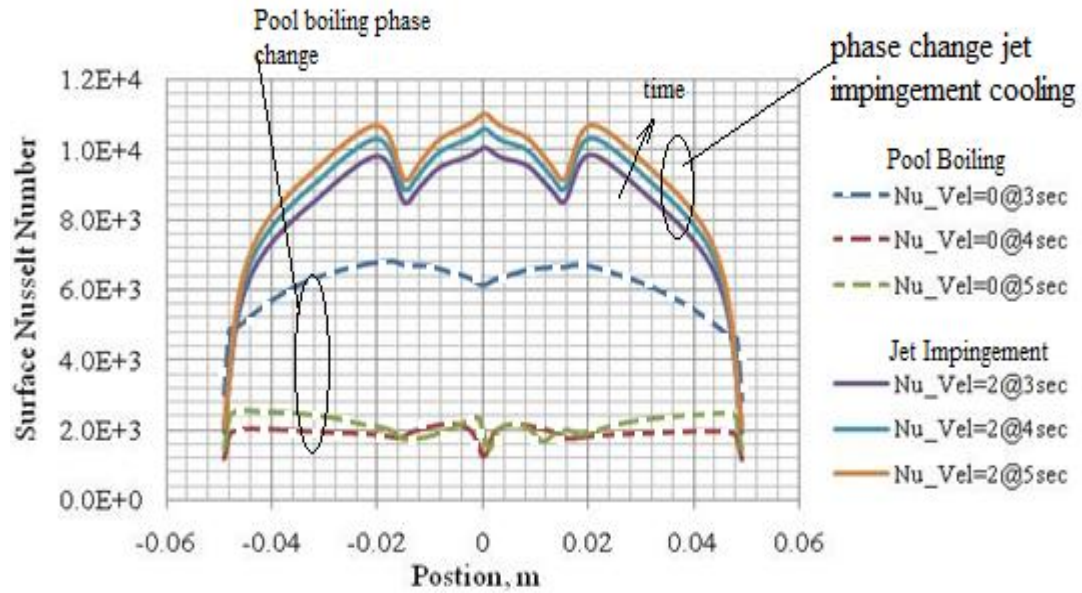


Figure 27. Surface Heat Flux comparison



**Figure 28. Surface Nusselt Number comparison**

The comparison contour plot shown in Figure 29 is of volume fraction at different time elapse between pool boiling and jet impingement. The no jet flow simulations are shown on the left and the phase change with jet flow simulation are shown in the right hand column. The results show vapor plumes generated as a result of boiling phenomena occurring at the bottom wall in the left column. On the other hand when the jet is applied, the vapor is confined to a relatively small region close to the bottom wall and side walls. The vapor is seen to accumulate in the corners where the flow is minimal. The result indicate that phase change with jet impingement provides a significant improvement on the heat flux profile. Compared to Figure 21, the heat flux spikes at  $\pm 0.015$  distance from the center are eliminated when phase change is introduced. Further investigation is needed to resolve the phase change process at the interface.



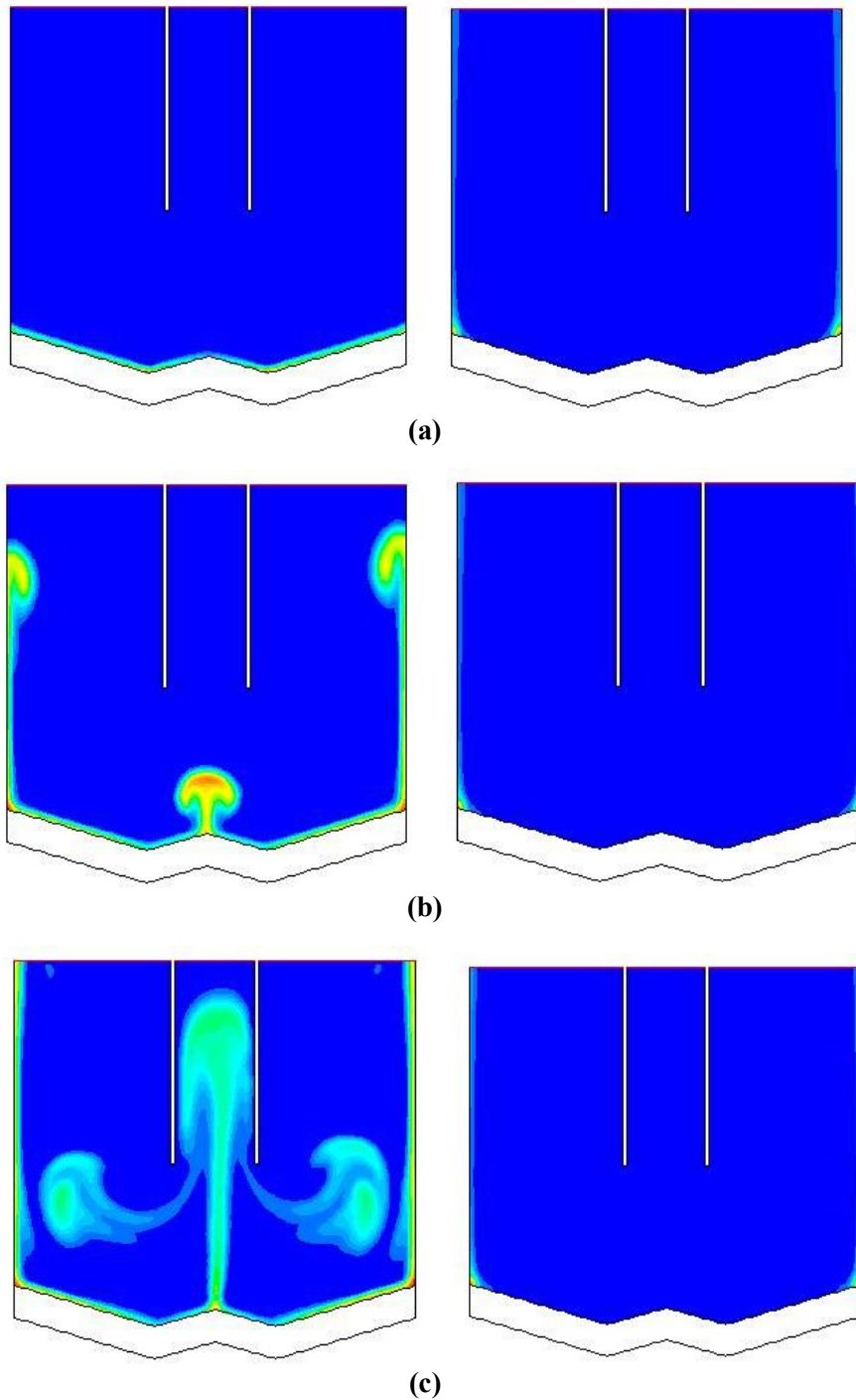


**Figure 29.** Contours of volume fraction of vapor (a)  $t=3\text{sec}$ , (b)  $t=4\text{sec}$ , and (c)  $t=5\text{sec}$  for pool phase change model (left) and jet impingement model with jet velocity of 2 m/s (right)

## **CHAPTER 5**

### **CONCLUSION**

CFD models developed in the present study provide tools to assess single phase and two-phase cooling schemes which may be difficult to resolve using experimental methods. The UDF developed extended the usefulness of Fluent® software in heat transfer by adding the phase change physics. However writing and compiling a UDF code requires a higher level programming and debugging skill since the physics of the phase process is still under development by the research community.

The phase change jet impingement cooling process produces the best heat transfer enhancement for high rate heat flux components. However, as comparisons between a pool boiling and jet impingement shows, two-phase cooling effect is more pronounced for a natural convection mode than for jet impingement scheme. The reason is jet impingement itself is more effective than phase change in stagnate pool removing heat from a substrate. Modifying the impingement surface from flat to the constructed V-type model, results in an overall heat flux enhancement of 13.35%. Additional modification of the impingement surface to the new shape (VA model) constructed by overlaying the two wedge angles that gave better regional performances, the overall heat flux is increased by 20%.

This study also identified that phase change has a saturation point in jet impingement cooling scheme. Liquid jet pushes the impingement surface boundary later

to a very small thickness and to the corners where flow separation exists. However incorporating phase change at the corners increase the surface heat transfer rate for the fact that heat transfer is enhanced due to phase change process where fluid motion is minimal. The effect can be explained by boundary layer reduction due to presence of jet flow.

Further study can be performed using the generated model for vapor atomized spray cooling technique instead of a single phase liquid jet. The exhaustive literature review performed in chapter 2 confirmed that spray cooling has a better performance and few more advantages than jet impingement. Therefore, it is beneficiary to see the effect of using vapor assisted spray cooling than jet impingement on the overall heat transfer. It is also ambiguous to tell the exact physics when phase change is applied to the jet impingement process therefore further study needs to be done on that topic as well.



## REFERENCES

1. Bergles, A. E., (1998). "Techniques to enhance heat transfer." in Handbook of Heat Transfer, Rohsenow, W. M., Hartnett, J. P., Cho, Y. I., eds., McGraw-Hill, New York, 11.1-11.76.
2. Colucci, D. W. and R. Viskanta (1996). "Effect of nozzle geometry on local convective heat transfer to a confined impinging air jet." *Experimental Thermal and Fluid Science* 13(1): 71-80.
3. Li, B. Q., T. Cader, et al. (2006). "Spray angle effect during spray cooling of microelectronics: Experimental measurements and comparison with inverse calculations." *Applied Thermal Engineering* 26(16): 1788-1795.
4. Peper, F., W. Leiner, et al. (1997). "Impinging radial and inline jets: A comparison with regard to heat transfer, wall pressure distribution, and pressure loss." *Experimental Thermal and Fluid Science* 14(2): 194-204.
5. Piroo, I. L., W. Rohsenow, et al. (2004). "Nucleate pool-boiling heat transfer. I: review of parametric effects of boiling surface." *International Journal of Heat and Mass Transfer* 47(23): 5033-5044.
6. Piroo, I. L., W. Rohsenow, et al. (2004). "Nucleate pool-boiling heat transfer. II: assessment of prediction methods." *International Journal of Heat and Mass Transfer* 47(23): 5045-5057.
7. Silk, E. A., J. Kim, et al. (2006). "Spray cooling of enhanced surfaces: Impact of structured surface geometry and spray axis inclination." *International Journal of Heat and Mass Transfer* 49(25-26): 4910-4920.
8. Puschmann, F. and E. Specht (2004). "Transient measurement of heat transfer in metal quenching with atomized sprays." *Experimental Thermal and Fluid Science* 28(6): 607-615.
9. Bernardin, J. D. and I. Mudawar (1997). "Film boiling heat transfer of droplet streams and sprays." *International Journal of Heat and Mass Transfer* 40(11): 2579-2593.
10. Kim, J. (2007). "Spray cooling heat transfer: The state of the art." *International Journal of Heat and Fluid Flow* 28(4): 753-767.
11. Mal, A. K., C. C. Yin, et al. (1991). "Ultrasonic nondestructive evaluation of cracked composite laminates." *Composites Engineering* 1(2): 85-101.

12. San, J.-Y., Y.-M. Tsou, et al. (2007). "Impingement heat transfer of staggered arrays of air jets confined in a channel." *International Journal of Heat and Mass Transfer* 50(19-20): 3718-3727.
13. Omar, A. M. T., M. S. Hamed, et al. "Modeling of nucleate boiling heat transfer under an impinging free jet." *International Journal of Heat and Mass Transfer In Press*, Corrected Proof.
14. Liu, H. M. (1997). "Numerical modeling of gas atomization in the spray forming process." *Journal of Materials Synthesis and Processing* 5(1): 11-17.
15. Behnia, M., S. Parneix, et al. (1999). "Numerical study of turbulent heat transfer in confined and unconfined impinging jets." *International Journal of Heat and Fluid Flow* 20(1): 1-9.
16. Bernardin, J. D., C. J. Stebbins, et al. (1997). "Mapping of impact and heat transfer regimes of water drops impinging on a polished surface." *International Journal of Heat and Mass Transfer* 40(2): 247-267.
17. Anglart, H., O. Nylund, et al. (1997). "CFD prediction of flow and phase distribution in fuel assemblies with spacers." *Nuclear Engineering and Design* 177(1-3): 215-228.
18. Garimella, S. V. and B. Nenaydykh (1996). "Nozzle-geometry effects in liquid jet impingement heat transfer." *International Journal of Heat and Mass Transfer* 39(14): 2915-2923.
19. Mitrovic, J. "Formation of a liquid jet after detachment of a vapour bubble." *International Journal of Heat and Mass Transfer* 40(18): 4309-4317.
20. Mitrovic, J. (2006). "How to create an efficient surface for nucleate boiling?" *International Journal of Thermal Sciences* 45(1): 1-15.
21. Timm, W., K. Weinzierl, et al. (2003). "Heat transfer in subcooled jet impingement boiling at high wall temperatures." *International Journal of Heat and Mass Transfer* 46(8): 1385-1393.
22. Kamnis, S. and S. Gu (2005). "Numerical modelling of droplet impingement." *Journal of Physics D-Applied Physics* 38(19): 3664-3673.
23. Brignoni, L. A. and S. V. Garimella (2000). "Effects of nozzle-inlet chamfering on pressure drop and heat transfer in confined air jet impingement." *International Journal of Heat and Mass Transfer* 43(7): 1133-1139.
24. Wendelstorf, J., K. H. Spitzer, et al. (2008). "Spray water cooling heat transfer at high temperatures and liquid mass fluxes." *International Journal of Heat and Mass Transfer* 51(19-20): 4902-4910.

25. Chizhov, A. V. and K. Takayama (2004). "The impact of compressible liquid droplet on hot rigid surface." *International Journal of Heat and Mass Transfer* 47(6-7): 1391-1401.
26. Wolf, D. H., F. P. Incropera, et al. (1996). "Local jet impingement boiling heat transfer." *International Journal of Heat and Mass Transfer* 39(7): 1395-1406.
27. Estes, K. A. and I. Mudawar (1995). "Correlation of sauter mean diameter and critical heat flux for spray cooling of small surfaces." *International Journal of Heat and Mass Transfer* 38(16): 2985-2996.
28. Collin, A., P. Boulet, et al. (2008). "Dynamics and thermal behaviour of water sprays." *International Journal of Thermal Sciences* 47(4): 399-407.
29. Moreira, A. L. N. and M. R. O. Panão (2006). "Heat transfer at multiple-intermittent impacts of a hollow cone spray." *International Journal of Heat and Mass Transfer* 49(21-22): 4132-4151.
30. Jia, W. and H. H. Qiu (2003). "Experimental investigation of droplet dynamics and heat transfer in spray cooling." *Experimental Thermal and Fluid Science* 27(7): 829-838.
31. Goodro, M., J. Park, et al. (2007). "Effects of Mach number and Reynolds number on jet array impingement heat transfer." *International Journal of Heat and Mass Transfer* 50(1-2): 367-380.
32. Grant, P. S., B. Cantor, et al. (1993). "Modeling of droplet dynamic and thermal histories during spray forming .1. Individual droplet behavior." *Acta Metallurgica Et Materialia* 41(11): 3097-3108.
33. Gulati, P., V. Katti, et al. (2009). "Influence of the shape of the nozzle on local heat transfer distribution between smooth flat surface and impinging air jet." *International Journal of Thermal Sciences* 48(3): 602-617.
34. Rahimi, M., I. Owen, et al. (2003). "Impingement heat transfer in an under-expanded axisymmetric air jet." *International Journal of Heat and Mass Transfer* 46(2): 263-272.
35. Chatzikyriakou, D., S. P. Walker, et al. (2009). "Comparison of measured and modelled droplet-hot wall interactions." *Applied Thermal Engineering* 29(7): 1398-1405.
36. Zhao, Z., D. Poulikakos, et al. (1996). "Heat transfer and fluid dynamics during the collision of a liquid droplet on a substrate--I. Modeling." *International Journal of Heat and Mass Transfer* 39(13): 2771-2789.

37. Woodfield, P. L., M. Monde, et al. (2005). "Observations of high temperature impinging-jet boiling phenomena." *International Journal of Heat and Mass Transfer* 48(10): 2032-2041.
38. Chen, R.-H., L. C. Chow, et al. (2004). "Optimal spray characteristics in water spray cooling." *International Journal of Heat and Mass Transfer* 47(23): 5095-5099.
39. Mozumder, A. K., M. Monde, et al. (2005). "Delay of wetting propagation during jet impingement quenching for a high temperature surface." *International Journal of Heat and Mass Transfer* 48(25-26): 5395-5407.
40. Buyevich, Y. A. and V. N. Mankevich (1996). "Cooling of a superheated surface with a jet mist flow." *International Journal of Heat and Mass Transfer* 39(11): 2353-2362.
41. Fitzgerald, J. A. and S. V. Garimella "A study of the flow field of a confined and submerged impinging jet." *International Journal of Heat and Mass Transfer* 41(8-9): 1025-1034.
42. Baydar, E. (1999). "Confined impinging air jet at low Reynolds numbers." *Experimental Thermal and Fluid Science* 19(1): 27-33.
43. Lin, L. and R. Ponnappan (2003). "Heat transfer characteristics of spray cooling in a closed loop." *International Journal of Heat and Mass Transfer* 46(20): 3737-3746.
44. Horacek, B., K. T. Kiger, et al. (2005). "Single nozzle spray cooling heat transfer mechanisms." *International Journal of Heat and Mass Transfer* 48(8): 1425-1438.
45. Tong, W., A. Bar-Cohen, et al. (1990). "Contact angle effects on boiling incipience of highly-wetting liquids." *International Journal of Heat and Mass Transfer* 33(1): 91-103.
46. Lee, J. (2009). "Role of Surface Roughness in Water Spray Cooling Heat Transfer of Hot Steel Plate." *Isij International* 49(12): 1920-1925.
47. Pasandideh-Fard, M., S. D. Aziz, et al. (2001). "Cooling effectiveness of a water drop impinging on a hot surface." *International Journal of Heat and Fluid Flow* 22(2): 201-210.
48. Oliveira, M. S. A. and A. C. M. Sousa (2001). "Neural network analysis of experimental data for air/water spray cooling." *Journal of Materials Processing Technology* 113(1-3): 439-445.

49. Katti, V. and S. V. Prabhu (2008). "Heat transfer enhancement on a flat surface with axisymmetric detached ribs by normal impingement of circular air jet." *International Journal of Heat and Fluid Flow* 29(5): 1279-1294.
50. Bhattacharya, P., A. N. Samanta, et al. (2009). "Spray evaporative cooling to achieve ultra fast cooling in runout table." *International Journal of Thermal Sciences* 48(9): 1741-1747.
51. Wang, T., J. L. Gaddis, et al. (2005). "Mist/steam heat transfer of multiple rows of impinging jets." *International Journal of Heat and Mass Transfer* 48(25-26): 5179-5191.
52. Li, X., J. L. Gaddis, et al. (2003). "Mist/steam cooling by a row of impinging jets." *International Journal of Heat and Mass Transfer* 46(12): 2279-2290.
53. Panão, M. R. O. and A. L. N. Moreira (2009). "Heat transfer correlation for intermittent spray impingement: A dynamic approach." *International Journal of Thermal Sciences* 48(10): 1853-1862.
54. Panão, M. R. O. and A. L. N. Moreira (2005). "Thermo- and fluid dynamics characterization of spray cooling with pulsed sprays." *Experimental Thermal and Fluid Science* 30(2): 79-96.
55. Rittidech, S., N. Pipatpaiboon, et al. (2007). "Heat-transfer characteristics of a closed-loop oscillating heat-pipe with check valves." *Applied Energy* 84(5): 565-577.
56. Cornaro, C., A. S. Fleischer, et al. (1999). "Flow visualization of a round jet impinging on cylindrical surfaces." *Experimental Thermal and Fluid Science* 20(2): 66-78.
57. Katti, V. and S. V. Prabhu (2008). "Experimental study and theoretical analysis of local heat transfer distribution between smooth flat surface and impinging air jet from a circular straight pipe nozzle." *International Journal of Heat and Mass Transfer* 51(17-18): 4480-4495.
58. O'Donovan, T. S. and D. B. Murray (2008). "Fluctuating fluid flow and heat transfer of an obliquely impinging air jet." *International Journal of Heat and Mass Transfer* 51(25-26): 6169-6179.
59. Afzal, N. "Falkner-Skan equation for flow past a stretching surface with suction or blowing: Analytical solutions." *Applied Mathematics and Computation* In Press, Corrected Proof.
60. Fluent manual, 2006

61. Islam, M. A., M. Monde, et al. (2008). "Jet impingement quenching phenomena for hot surfaces well above the limiting temperature for solid-liquid contact." *International Journal of Heat and Mass Transfer* 51(5-6): 1226-1237.
62. Rubinstein, L.I. "The Stefan problem," *Amer. Math. Soc.* (1971) (Translated from Russian)

## APPENDIX A

### PHASE CHANGE HEAT TRANSFER THEORY

Substantial derivative for two-dimensional case, is given as  $\frac{D}{Dt} = \frac{\partial}{\partial t} + u \frac{\partial}{\partial x} + v \frac{\partial}{\partial y}$

The Laplacian for 2D flow is defined as  $\nabla^2 = \frac{\partial^2}{\partial x^2} + \frac{\partial^2}{\partial y^2}$

$$\frac{\partial H}{\partial t} + u \frac{\partial H}{\partial x} + v \frac{\partial H}{\partial y} = K \left( \frac{\partial^2 T}{\partial x^2} + \frac{\partial^2 T}{\partial y^2} \right)$$

$$\frac{\partial H}{\partial t} = \frac{\partial H}{\partial T} \times \frac{\partial T}{\partial t}$$

Similarly

$$\frac{\partial H}{\partial x} = \frac{\partial H}{\partial T} \times \frac{\partial T}{\partial x} \quad \text{and} \quad \frac{\partial H}{\partial y} = \frac{\partial H}{\partial T} \times \frac{\partial T}{\partial y}$$

Substituting these into the general enthalpy equation gives a temperature dependent energy equation with a subscript  $i$ , for the region in consideration

$$\left( \rho C_p + \frac{\rho h_{fg}}{T_{sat}} \right)_i \frac{\partial T}{\partial t} + u \left( \rho C_p + \frac{\rho h_{fg}}{T_{sat}} \right)_i \frac{\partial T}{\partial x} + v \left( \rho C_p + \frac{\rho h_{fg}}{T_{sat}} \right)_i \frac{\partial T}{\partial y} = K_i \left( \frac{\partial^2 T}{\partial x^2} + \frac{\partial^2 T}{\partial y^2} \right)$$

Three regions have to be solved together to get a well poised expression and a converged solution.

Pure liquid region:  $T < T_{sat}$

$$(\rho C_p)_l \frac{\partial T}{\partial t} + u (\rho C_p)_l \frac{\partial T}{\partial x} + v (\rho C_p)_l \frac{\partial T}{\partial y} = K_l \left( \frac{\partial^2 T}{\partial x^2} + \frac{\partial^2 T}{\partial y^2} \right)$$

Interface boundary, Stefan condition:  $T = T_{sat}$

$$\left(\frac{\rho h_{fg}}{T_{sat}}\right) \frac{\partial T}{\partial t} + u \left(\frac{\rho h_{fg}}{T_{sat}}\right) \frac{\partial T}{\partial x} + v \left(\frac{\rho h_{fg}}{T_{sat}}\right) \frac{\partial T}{\partial y} = K \left(\frac{\partial^2 T}{\partial x^2} + \frac{\partial^2 T}{\partial y^2}\right)$$

This expression is also called Stefan condition (Rubinstein L. I. [62])

Pure vapor region:  $T > T_{sat}$

$$(\rho C_p)_v \frac{\partial T}{\partial t} + u (\rho C_p)_v \frac{\partial T}{\partial x} + v (\rho C_p)_v \frac{\partial T}{\partial y} = K_v \left(\frac{\partial^2 T}{\partial x^2} + \frac{\partial^2 T}{\partial y^2}\right)$$

Phase change heat transfer is a rather complicated process. At point in time, the liquid that comes in contact with the heated surface absorb the sensible heat and its temperature increases. As the temperature adjacent to the heated surface increases above the fluid saturation temperature, phase change start to occur, [see literature review]. As a result, the portion of fluid that undergoes phase change takes a significant amount of heat from the surface. Gradually, a vapor film start to accumulate around the heated surface until enough amount of vapor coalesces to be lifted up by buoyancy effect. The insulating vapor film at the heated surface also acts as a heat transfer medium just like the liquid layer but with a much lower thermal conductivity coefficient. Therefore, some part of the heated surface will be in contact with liquid and some with vapor, in addition a phase change takes place simultaneously. Thus to effectively solve this problem the famous Stefan relation is solved for the three different temperature zones jointly.

Consider a pool of liquid at constant temperature  $T_o < T_{sat}$ , occupying a semi-infinite region  $x \geq 0$ .  $T_{sat}$  is the saturation temperature where the liquid start to boil or change its phase. At  $T_{sat}$ , which is also known as equilibrium phase change temperature, liquid and vapor phases can co-exist in thermodynamic equilibrium. But as the heated surface temperature exceeds  $T_{sat}$  at  $x = 0$  the liquid starts changing its phase. For any



time  $t$ , the overall region consists of liquid and vapor phases with liquid phase occupying the region  $0 \leq x < \infty$  and vapor takes the region  $X(t) \leq x < \infty$ .  $X(t)$  is the demarcating interface for the two phases or the free boundary.

In liquid zone:

$$C_l \rho_l \frac{\partial T_l}{\partial t} = K_l \frac{\partial^2 T_l}{\partial x^2}; \quad t > 0 \text{ and } 0 < X(t)$$

$$T_l(x, y, t) \Big|_{x=0} = T_b < T_{sat}; \quad t > 0$$

In vapor region

$$C_v \rho_v \frac{\partial T_v}{\partial t} + C_v \rho_v u \frac{\partial T_v}{\partial x} = K_v \frac{\partial^2 T_v}{\partial x^2}; \quad t > 0 \text{ and } X(t) < x < \infty$$

$$T_v(x, y, t) \Big|_{t=0} = T_o; \quad T_v(x, y, t) \Big|_{x \rightarrow \infty} = T_o;$$

At the boundary  $x = X(t)$

$$T_l = T_v = T_{sat}$$

$$K_l \frac{\partial T_l}{\partial x} - K_v \frac{\partial^2 T_v}{\partial x^2} = \{h_{fg} \rho_l + (C_v \rho_v - C_l \rho_l) T_{sat}\} \frac{dX}{dt} \quad t > 0 \text{ and } 0 < X(t)$$

$$S(0) = 0$$

## APPENDIX B

### DIFFERENT IMPINGEMENT SURFACES

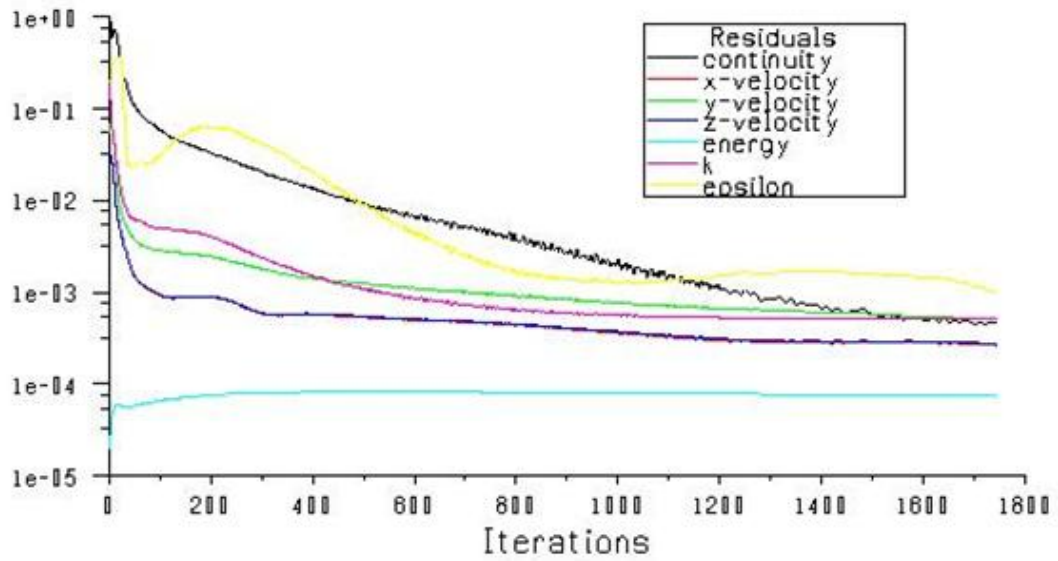


Figure B1. Convergence criteria by monitoring equation residuals

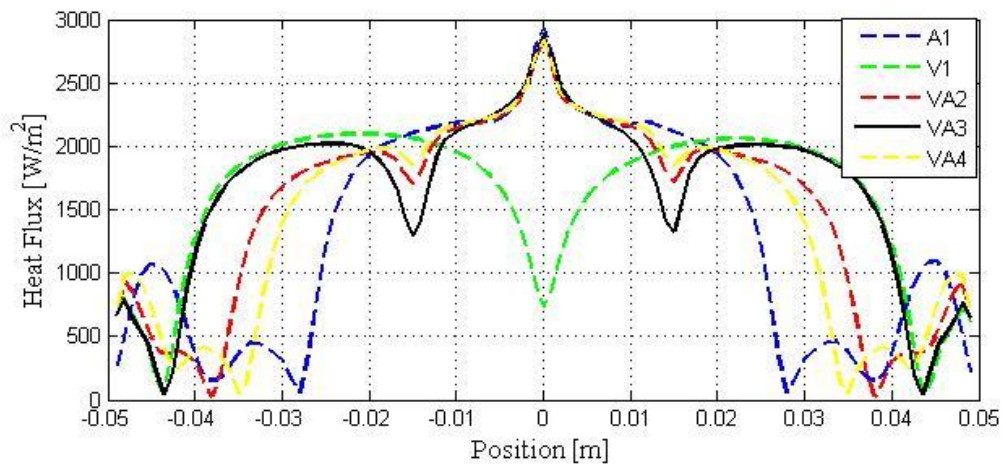
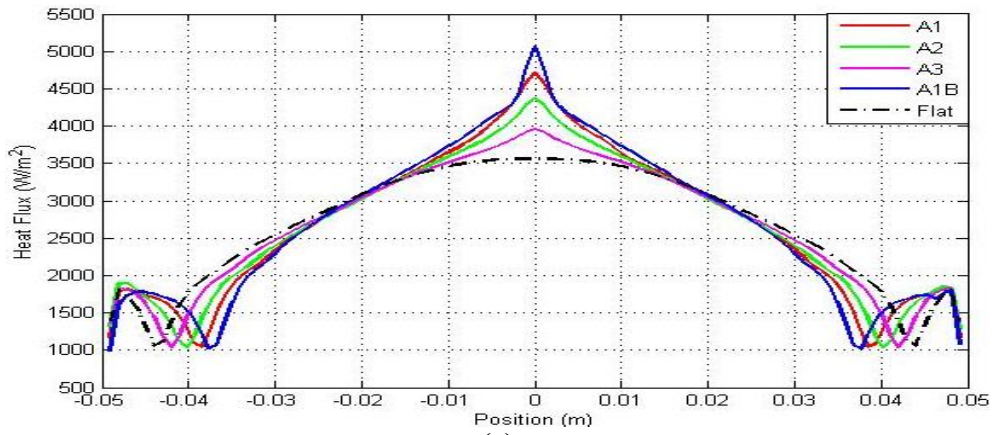
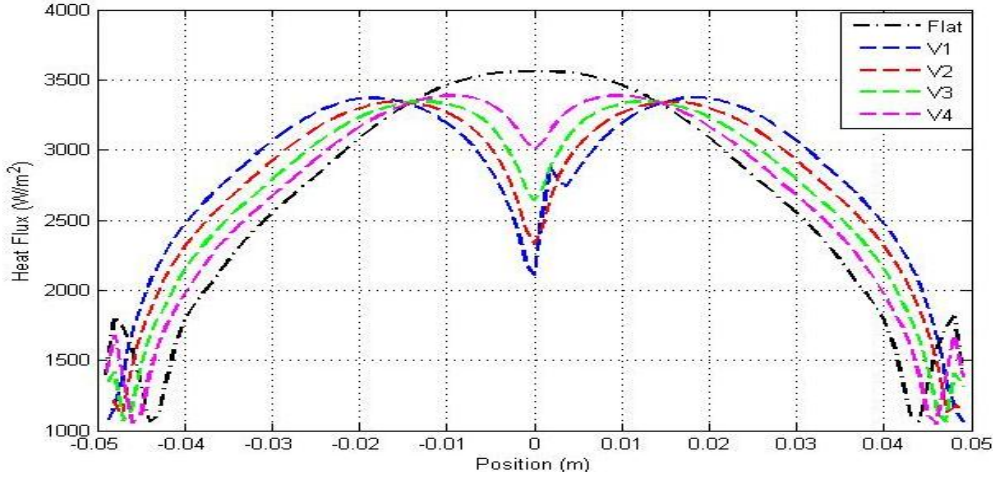


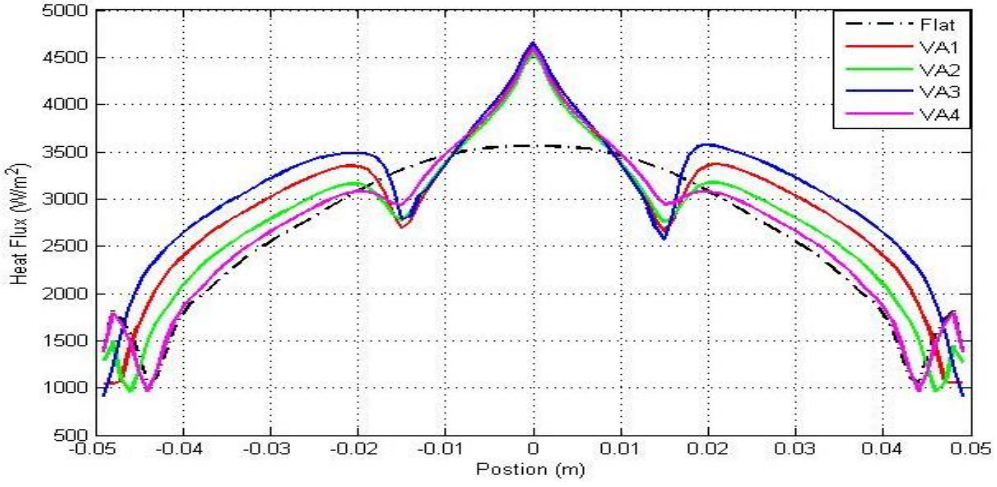
Figure B2. Heat Flux comparison of the different models



(a)



(b)



(c)

**Figure B3. Heat Flux comparison for (a) A-type (b) V-type and (c) VA-type models**

Area under the curve is calculated using trapezoidal method in Matlab using [trapz(x,y) command] which gives the values tabulated in Table B1, for the different models.

**Table B1. Area under surface heat flux curve**

Model Type	Heat Flux Area under curve [W]	Area % Increase	Heat Flux (W/m <sup>2</sup> )		
			at Stagnation	at 0.03m	at corner
<b>A0 (A0)</b>	268.48	1.948	5071.78	2300.01	988.536
<b>A1</b>	266.95	1.386	4710.22	2373.8	1175.51
<b>A2</b>	264.98	0.653	4372.41	2408.92	1318.66
<b>A3</b>	263.45	0.076	3961.07	2470.7	1370.91
<b>Flat</b>	263.25	0.0	3558.62	2546.96	1397.84
<b>V1</b>	277.27	5.056	2109.99	3060.8	1045.75
<b>V2</b>	271.71	3.114	2325.68	2930.9	1210.25
<b>V3</b>	267.35	1.534	2639.22	2786.33	1318.92
<b>V4</b>	264.43	0.446	3004.98	2673.09	1380.22
<b>VA3</b>	307.36	14.351	4659.6	3221.72	913.175
<b>VA1</b>	290.16	9.274	4627.57	3028.33	1043.96
<b>VA2</b>	276.19	4.685	4553.46	2801.58	1275.55
<b>VA4</b>	271.28	2.960	4591.28	2657.28	1385.47

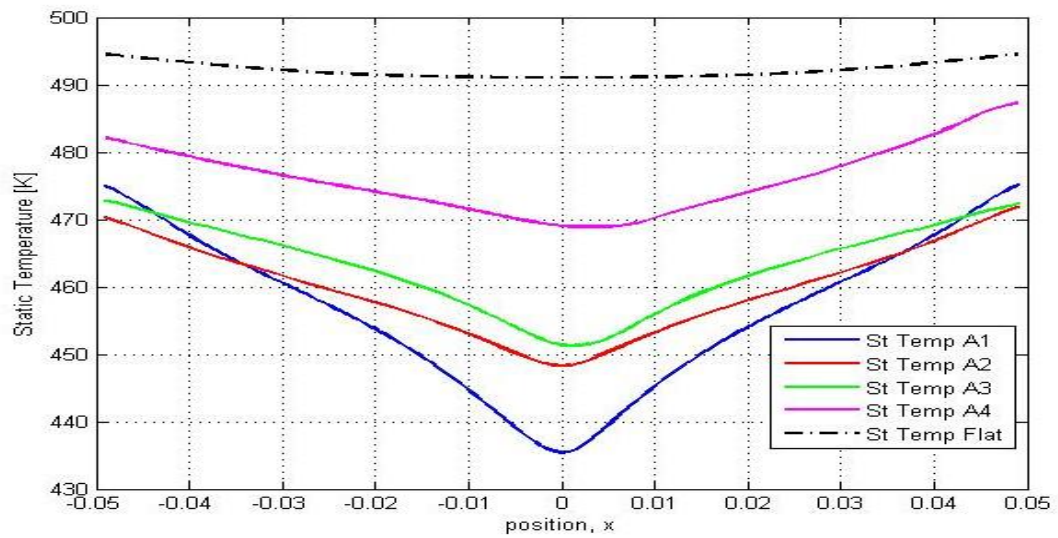


**Figure B4. Steady state temperature comparison for A-type model**

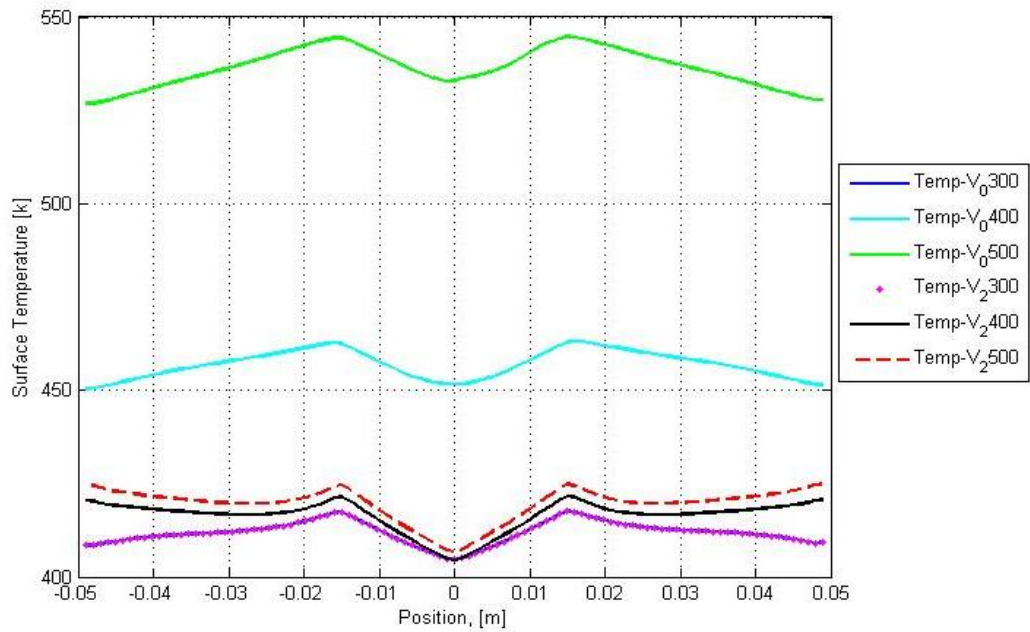


**Figure B5. Surface temperature profile for pool boiling and jet impingement**